# 1

# Statistical State Dynamics: a new perspective on turbulence in shear flow

B. F. FARRELL AND P. J. IOANNOU

## 1.1 Introduction

Adopting the perspective of statistical state dynamics (SSD) as an alternative to the traditional perspective afforded by the dynamics of sample state realizations has facilitated a number of recent advances in understanding turbulence in shear flow. SSD reveals the operation in shear flow turbulence of previously obscured mechanisms, particularly mechanisms arising from cooperative interaction among disparate scales in the turbulence. These mechanisms provide physical explanation for specific phenomena including formation of coherent structures in the turbulence as well as more general and fundamental insights into the maintenance and equilibration of the turbulent state. Moreover, these cooperative mechanisms and the phenomena associated with them are not amenable to analysis by the traditional method of studying turbulence using sample state dynamics. Another advantage of the SSD approach is that adopting the probability density function (pdf) as a state variable provides direct access to all the statistics of the turbulence, at least within the limitations of the approximations applied to the dynamics. Although the utility of obtaining the pdf directly as a state variable is obvious the pdf is often difficult to obtain accurately by sampling state trajectories even if the pdf is stationary. In the event that the pdf is time dependent, which is often the case, solving directly for the pdf as a state variable is the only alternative. While these are all important advantages afforded by adopting the pdf as a state variable, the overarching advantage is that adopting the statistical state as the dynamical variable allows an understanding of turbulence at a deeper level, which is the level in which the essential cooperative mechanisms underlying the turbulent state are manifest.

In this review one implementation of the SSD approach, referred to as Stochastic Structural Stability Theory (S3T) (equivalently CE2), will be introduced and some example applications described. In these applications S3T is used to study barotropic and baroclinic turbulence in planetary atmospheres, drift wave turbulence in plasmas, and the turbulence of wall-bounded shear flows. In each of these examples the S3T system is found to support turbulence with substantially the same statistical and dynamical structure as that simulated using the dynamical system underlying the turbulence (e.g. the Navier-Stokes (NS) equations in the case of wall-bounded shear turbulence), while providing insights into mechanism that can only be obtained through using the statistical state dynamics approach.

It is well accepted that complex spatially and temporally varying fields arising in physical systems characterized by chaos and involving interactions over an extensive range of scales in space and time can be insightfully analyzed using statistical variables. In the study of turbulent systems, examining statistical measures for variables arising in the turbulence is a common practice; however, it is less common to adopt statistical state variables for the dynamics of the turbulent system. The potential of SSD to provide insight into the mechanisms underlying turbulence has been largely overlooked in part because obtaining the dynamics of the statistical state has been assumed to be prohibitively difficult in practice. An early attempt to use SSD in the study of turbulence was the formal expansion in cumulants by Hopf (Hopf, 1952; Frisch, 1995). However Hopf's cumulant method was subsequently restricted in application, in large part due to the difficulty of obtaining robust closure of the expansion. Another familiar example of a theoretical application of SSD to turbulence is provided by the Fokker-Planck equation which, while very useful conceptually, is generally intractable for representing complex system dynamics except under very restrictive circumstances. Because of the perceived difficulty of implementing SSD to study systems of the type typified by turbulent flows, the dynamics of these systems has been most often explored by simulating sample state trajectories which are then analyzed to obtain an approximation to the assumed statistically steady probability density function of the turbulent state. This approach fails to provide insight into phenomena that are associated intrinsically with the dynamics of the statistical state rather than with the dynamics of sample realizations. The reason is that while the influence of multiscale cooperative phenomena on the statistical steady state of turbulence is apparent from the statistics of sample realizations, the cooperative phenomena producing these statistical equilibria have analytical expression only in the SSD of the associated system. It follows that in order to gain understanding of turbulent equilibria adopting the SSD perspective is essential. But there is a more subtle insight into the dynamics of turbulence afforded by the perspective of statistical state dynamics: while the statistical state of a turbulent system may asymptotically approach a fixed point, in which case the mean statistics gathered from sample realizations form a valid representation of the stationary statistical state, the dynamics of the statistical state may instead be time depen-

dent or even chaotic in which case the statistics of sample realizations do not form a valid comprehensive representation of the statistical state at any time. The dynamics of such turbulent systems is accessible to analysis only through its SSD.

Before introducing some illustrative examples of phenomena accessible to analysis through the use of SSD it is useful to inquire further as to why this method has not been more widely exploited heretofore. In fact, closure of cumulant expansions to obtain equilibria of the SSD has been very extensively studied in association with isotropic homogeneous turbulence (Kraichnan, 1959; Orszag, 1977; Rose and Sulem, 1978). However, the great analytical challenges posed by this approach and the limited success obtained using it served to redirect interest toward dimensional analysis and interpretation of simulations as a more promising approach to understanding the inertial subrange. It turns out that the inertial subrange, while deceptively straightforward in dynamical expression, is intrinsically and essentially nonlinear and as a result presents great obstacles to analysis. However, the arguably more relevant forms of turbulence, at least in terms of applications to meteorology, oceanography, MHD, and engineering fluid dynamics, is turbulence in shear flow at high Reynolds number. At the core of these manifestations of turbulence lies a dominant linear dynamics which is revealed by linearization about the mean shear itself. This linearization in turn uncovers an underlying simplicity of the dynamics arising from the high degree of non-normality of the linear operator associated with the mean shear which greatly limits both the set of dynamically relevant structures and their interaction with the mean shear. While not sufficient to eliminate the role of nonlinearity in the dynamics of turbulence entirely, these physical principles result in an essential dynamics of turbulence reduced to quasi-linear interaction between a restricted set of structures and the mean flow that supports them. For our purposes a primary implication of this naturally occurring dynamical restriction is that the SSD of shear flow turbulence is amenable to study using straightforward closures.

Consider the large scale jets that are prominent features of planetary scale turbulence in geophysical flows of which the banded winds of Jupiter and the Earth's polar jets are familiar examples. These jets can be divided into two groups: forced jets and free jets. Jupiter's jets are maintained by energy from turbulence excited by convection arising from heat sources in the planet's interior, and so the turbulence from which the jet arises may be regarded as dynamically independent of the jet structure itself. In contrast, the Earth's polar jets are maintained by turbulence arising from baroclinic growth processes drawing on the potential energy associated with the pole-equator temperature gradient. These baroclinic growth mechanisms depend strongly on jet structure. It follows that the mechanism producing the jet can not be separated dynamically from the mechanism producing the turbulence so that these problems must be solved together. In the case of Jupiter's jets the energy source is known from observations of the convection (Ingersoll, 1990) leaving two fundamental problems presented by the existence of these jets. The first is to explain how the jets arise from the turbulence and the second how they are equilibrated with the observed structure and maintained with this structure over time scales long compared with the intrinsic time scales of the turbulence. Although these phenomena manifest prominently in simulations of sample state realizations, neither is accessible to analysis using sample state simulation while both have analytical expression and straightforward solution when expressed using SSD (Farrell and Ioannou, 2003, 2007). Moreover, in the course of solving the SSD problem for jet formation and equilibration a set of subsidiary results are obtained including identification of the physical mechanism of jet formation (Bakas and Ioannou, 2013b), finite amplitude jet equilibration, and prediction of the existence of unexpected multiple equilibria jet states (Farrell and Ioannou, 2007, 2009a; Parker and Krommes, 2013; Constantinou et al., 2014) But perhaps most significant is the insight obtained from these statistical state equilibria into the nature of turbulence: the turbulent state is revealed to be fundamentally determined by cooperative interaction acting directly between large energy bearing scales and the small scales of the turbulence. This fundamental quasi-linearity, which is revealed by SSD, is a general property of turbulence in shear flow and it provides both conceptual clarity as well as analytical tractability to the turbulence closure problem.

In the case of free jets maintained by the baroclinic turbulence an additional issue arises: establishment of the statistical mean turbulent state in the case of supercritical imposed meridional temperature gradients requires equilibration of flow instability. Coincident with the equilibration of instability in supercritical baroclinic turbulence is a characteristic organization of the flow into planetary scale jets but this association remained an intriguing observation because analytic expression, much less solution, of the problem of flow instability equilibration is inaccessible within sample state dynamics of the associated baroclinic system. However, this problem can be directly solved using SSD: the equilibrium turbulent state is obtained in the form of fixed points of the SSD. Moreover, the mechanism of equilibration is also identified as these fixed points are found to be associated with stabilization of the supercritical flow by the jet structure, in large part by confinement of the perturbation modes by the jet structure to sufficiently small meridional scale that the instabilities are no longer supported, a mechanism previously referred to as the "barotropic governor" (Ioannou and Lindzen, 1986; James, 1987; Lindzen, 1993; Farrell and Ioannou, 2008, 2009c).

In the magnetic plasma confinement problem, which is of great importance to the quest for a practical fusion power source, the formation of jets by cooperative interaction with drift wave turbulence is fundamental to the effectiveness of the plasma confinement (Diamond et al., 2005). The dynamics of the jet-mediated high confinement regime is another example of a phenomenon that arises from cooperative interaction between scales in a turbulent flow and that can only be studied directly using SSD. Drift wave plasma turbulence, governed by the Hassagawa-Mima or Charney-Hasagawa-Mima equations, parallels in dynamics the baroclinic turbulence in the Earth's atmosphere with the Lorenz

force playing the role of the Coriolis force in the plasma case so it is not surprising that the same or very similar phenomena occur in these two systems. The time dependent statistical state of drift wave turbulence has natural expression as the trajectory of the statistical state evolving under its associated SSD. This trajectory commonly approaches a fixed point corresponding to a statistically steady state but in the case of plasma turbulence the statistical state commonly follows a limit cycle or even a chaotic trajectory. These time-dependent states are distinct conceptually from the familiar limit cycles or chaotic trajectories of sample state realizations. Rather, these statistical state trajectories represent time-dependence or chaos of the cooperative dynamics of the turbulence which, while apparent in observation of sample state temporal variability, has no counterpart in analysis based on sample state dynamics. Perhaps more familiar to the atmopheric science community is the example of a time-dependent statistical state trajectory provided by the limit cycle behavior of the Quasi-biennial Oscillation in the Earth's equatorial stratosphere (Farrell and Ioannou, 2003).

Another manifestation of turbulence is that collectively referred to as wall-bounded shear flow turbulence, examples of which include pressure driven pipe and channel flows, flow between differentially moving plane surfaces, that over airplane wings, and that of the convectively stable atmospheric boundary layer. These laminar shear flow velocity profiles have negative curvature and, consistent with the prediction of Rayleigh's theorem for their inviscid counterparts, these flows do not support inflectional instabilities. Two fundamental problems are posed by the turbulence occurring in wall-bounded shear flows: instigation of the turbulence, referred to as the bypass transition problem, and maintenance of the turbulent state once it has been established. The second of these problems, maintenance of turbulence in wall-bounded shear flow, is commonly associated with what is referred to as the Self-Sustaining Process (SSP). Transition can occur either by a pathway intrinsic to the SSD of the background turbulence or alternatively transition can be induced directly by imposition of a sufficiently large and properly configured state perturbation (Farrell and Ioannou, 2012). The former bypass transition mechanism has no analytical counterpart in sample state dynamics while the latter has been extensively studied using sample state realizations as for example in Brandt et al. (2004). While the bypass transition phenomenon can occur either by a mechanism analyzable using sample state dynamics or by an alternative mechanism that is analyzable only using SSD, the SSP mechanism maintaining the turbulent state is fundamentally a quasi-linear multiscale interaction amenable to analysis only by using SSD and it can be uniquely identified with a chaotic trajectory of the SSD of the flow (Farrell and Ioannou, 2012).

We describe below an implementation of SSD referred to as S3T in some detail (Farrell and Ioannou, 2003, 2007, 2008). S3T, which is alternatively referred to as the Second Order Cumulant Expansion (CE2) method (Srinivasan and Young, 2012) constitutes a closure of the dynamics at second order that results in a nonlinear autonomous dynamical system for the first two cumulants of the statistical mean state dynamics of the turbulence. This closure also forms the basis of recently proposed computational tools for climate simulations (Marston, 2012) and has recently been applied to problems such as macroscale barotropic and baroclinic turbulence in planetary atmospheres (Farrell and Ioannou, 2003, 2007, 2008; Marston et al., 2008; Farrell and Ioannou, 2009a,c; Marston, 2010; Bakas and Ioannou, 2011; Bakas and Ioannou, 2013b; Marston, 2012; Tobias et al., 2011; Srinivasan and Young, 2012; Constantinou et al., 2014), drift wave turbulence in plasmas (Farrell and Ioannou, 2009b,a), turbulence in wall-bounded shear flows (Farrell and Ioannou, 2012; Farrell et al., 2012) and astrophysical flows (Tobias et al., 2011).

## 1.2 Implementation of SSD: S3T theory and analysis

The S3T implementation for a given dynamical system is built on closure of the expansion in cumulants of the system dynamics (Hopf, 1952; Frisch, 1995). These cumulant equations govern the joint evolution of the mean flow (first cumulant) and the ensemble perturbation statistics (higher order cumulants). Closure is enforced by either a parameterization of the terms in the second cumulant equation that involve the third cumulant as stochastic excitation (Farrell and Ioannou, 1993a,b; DelSole and Farrell, 1996; DelSole, 2004b) or setting the third cumulant to zero (Marston et al., 2008; Tobias et al., 2011; Srinivasan and Young, 2012). These restrictions of the dynamics to the first two cumulants are equivalent to parameterizing or neglecting the perturbation-perturbation interactions in the fully non-linear dynamics respectively. The retained nonlinearity is the interaction between the perturbations with the instantaneous mean flow. This closure results in a non-linear, autonomous dynamical system that governs the evolution of the mean flow and its consistent second order perturbation statistics.

We now review the derivation of the S3T system starting from the discretized Navier-Stokes equations which can be assumed to take the generic form:

$$\frac{dx_i}{dt} = \sum_{j,k} a_{ijk} x_j x_k - \sum_j b_{ij} x_j + f_i \ . \tag{1.1}$$

The flow variable $x_i$ could be the velocity component at the $i$-th location of the flow and the discrete set of equations (1.1) could arise from discretization of the continuous fluid equations on a spatial grid. Any externally imposed body force is specified by $f_i$. In fluid systems $\sum_{i,j,k} a_{ijk} x_i x_j x_k$ vanishes identically and $\sum_{i,j} b_{ij} x_i x_j$ is positive definite in order that the system be dissipative. These two conditions imply that in the absence of dissipation and forcing $E = 1/2 \sum_i x_i^2$ is conserved.

Consider now the averaging operator $\overline{(\cdot)}$. This averaging operator could be the zonal mean in a planetary flow, but for now it is left unspecified. Decompose the variables into mean, and perturbation: $x_i = X_i + x_i'$, where $X_i \equiv \overline{x}_i$, and $f_i = F_i + f_i'$ and assume that $f_i'$ are stochastic while $F_i$ are

deterministic. The mean and perturbation variables evolve according to:

$$\frac{dX_i}{dt} - \sum_{j,k} a_{ijk} X_j X_k + \sum_j b_{ij} X_j = \sum_{j,k} a_{ijk} \overline{x'_j x'_k} + F_i, \tag{1.2a}$$

$$\frac{dx'_i}{dt} = \sum_j A_{ij}(X) x'_j + F^{nl}_i + f'_i, \tag{1.2b}$$

where

$$A_{ij}(X) = \sum_k \left( a_{ikj} + a_{ijk} \right) X_k - b_{ij} \ , \tag{1.3}$$

and

$$F^{nl}_i = \sum_{j,k} a_{ijk} \left( x'_j x'_k - \overline{x'_j x'_k} \right) \ . \tag{1.4}$$

The term $\sum_j A_{ij}(X) x'_j$ is bilinear in $X$ and $x'$ and represents the influence of the mean flow on the perturbation dynamics while the quadratically nonlinear term $F^{nl}$ represents the perturbation-perturbation interactions which are responsible for the turbulent cascade in the perturbation variables. The term $F^{rs}_i \equiv \sum_{j,k} a_{ijk} \overline{x'_j x'_k}$, in (1.2a) is the Reynolds stress divergence and represents the influence of the perturbations on the mean flow. Equations (1.2) determine the evolution of the mean flow and the perturbation variables under the full non-linear dynamics (1.1) and will be referred to as the NL equations.

The quasi-linear (QL) approximation to NL results when the perturbation-perturbation interactions (given by term $F^{nl}$ in (1.2b)) are either neglected entirely or replaced by a stochastic parameterization while the influence of perturbations on the mean is retained fully by incorporating the term $F^{rs}$ in the mean equation (1.2a). The QL approximation of (1.2) under the stochastic parameterization $F^{nl}_i + f'_i = \sqrt{\epsilon} \sum_j F_{ij} dB_{tj}$ is:

$$\frac{dX_i}{dt} - \sum_{j,k} a_{ijk} X_j X_k + \sum_j b_{ij} X_j = \sum_{j,k} a_{ijk} \overline{x'_j x'_k} + F_i, \tag{1.5a}$$

$$dx'_i = \sum_{j=1}^{n} A_{ij}(X) x'_j dt + \sqrt{\epsilon} F_{ij} \, dB_{tj}. \tag{1.5b}$$

The noise terms, $dB_{tj}$, are independent delta correlated infinitesimal increments of a one-dimensional Brownian motion at time $t$ (cf. Øksendal (2000)) satisfying:

$$\langle dB_{ti} \rangle = 0 \ , \ \left\langle dB_{ti} dB_{sj} \right\rangle = \delta_{ij} \delta(t-s) \, dt \ , \tag{1.6}$$

in which $\langle \cdot \rangle$ denotes the ensemble average over realizations of the noise. Equations (1.5) will be referred to as the QL equations. In the absence of forcing and dissipation the QL equations conserve the quantity $E^{ql} = \frac{1}{2} \sum_i \left( X_i^2 + x_i'^2 \right)$ and in the presence of bounded deterministic forcing, $F_i$, and dissipation realizations of the dynamics (1.5b) have all moments finite at all times. In general the quantity conserved in NL differs from that conserved in QL and their difference is $E - E^{ql} = \sum_i X_i x'_i$. This cross term vanishes under an appropriate choice of an averaging operator. For example if the averaging operator is the zonal mean and the index refers to the value of variable on a spatial grid the cross term vanishes and then $E = E^{ql}$. We will require that the averaging operator has the property that the QL invariants are the same as the NL invariants.

Consider $N$ realizations of the perturbation dynamics (1.5b) evolving under excitation by statistically independent realizations of the forcing but all evolving under the influence of a common mean flow $X$ according to

$$dx'^r_i = \sum_{j=1}^{n} A_{ij}(X) x'^r_j dt + \sqrt{\epsilon} F_{ij} dB^r_{tj}, \quad (r = 1, \ldots, N). \tag{1.7}$$

Denote with superscript $r$ the $r$-th realization so that $x^r_j(t)$ corresponds to the forcing $dB^r_{tj}$. Assume further that the mean flow $X$ is evolving under the influence of the average $F^{rs}$ over these $N$ realizations, so that:

$$\frac{dX_i}{dt} - \sum_{j,k} a_{ijk} X_j X_k + \sum_j b_{ij} X_j = \sum_{j,k} a_{ijk} \overline{C^N_{jk}} + F_i \ , \tag{1.8}$$

with

$$C^N_{ij} = \frac{1}{N} \sum_{r=1}^{N} x'^r_i x'^r_j \ , \tag{1.9}$$

the $N$-ensemble averaged perturbation covariance matrix. To motivate this ensemble consider the case in which the averaging operator is the zonal mean and assume that over a latitude circle the zonal decorrelation scale is such that the latitude circle may be considered to be populated by $N$ independent perturbation structures, all of which contribute additively to the Reynolds stresses that collectively contribute to maintain the zonal mean flow.

It is desirable to derive an explicit equation for the evolution of $C^N_{ij}$ in terms of $X$ and $C^N_{ij}$. To achieve this we obtain the differential equation for $C^N_{ij}$, which using the Itô lemma and (1.7) is:

$$\begin{aligned} dC^N_{ij} &= \frac{1}{N} \sum_{r=1}^{N} \left( dx'^r_i x'^r_j + x'^r_i dx'^r_j \right) + \epsilon \sum_{k=1}^{n} F_{ik} F^T_{kj} dt \\ &= \sum_{k=1}^{n} \left( A_{ik}(X) C^N_{kj} + C^N_{ik} A^T_{kj}(X) + \epsilon F_{ik} F^T_{kj} \right) dt + \\ &\quad + \frac{\sqrt{\epsilon}}{N} \sum_{r=1}^{N} \sum_{k=1}^{n} \left( F_{ik} x'^r_j + F_{jk} x'^r_i \right) dB^r_{tk} \ . \end{aligned} \tag{1.10}$$

The stochastic equation (1.10) should be understood in the Itô sense, so that the variables $x'$ and the noise $dB_t$ are uncorrelated in time and the ensemble mean of each of $\left( F_{ik} x'^r_j + F_{jk} x'^r_i \right) dB^r_{tk}$ vanishes at all times. The corresponding differential equation in the physically relevant Stratonovich interpretation is obtained by removing from equation (1.10) the term $\epsilon \sum_{k=1}^{n} F_{ik} F^T_{kj} \, dt$. However, both interpretations produce identical covariance evolutions because in the Stratonovich interpretation the mean of $\left( F_{ik} x'^r_j + F_{jk} x'^r_i \right) dB^r_{tk}$ is nonzero and equal exactly to the term $\epsilon \sum_{k=1}^{n} F_{ik} F^T_{kj} dt$ that was removed from the Itô equation. This results because the noise in (1.7) enters additively and the equations are linear. The noise term in

(1.10) can be further reduced using the Itô isometry (cf. Øksendal (2000)) according to which any noise of the form $\sum_{k=1}^{m} g_k(x'_1,\ldots,x'_n)\,dB_{tk}$ can be replaced by the single noise process $\sqrt{\sum_{k=1}^{m} g_k^2(x'_1,\ldots,x'_n)}\;dB_t$, in the sense that both processes have the same probability distribution function. Applying the Itô isometry to the noise terms in (1.10) we obtain

$$\frac{\sqrt{\epsilon}}{N}\sum_{r=1}^{N}\sum_{k=1}^{n}\left(F_{ik}x'^{r}_{j}+F_{jk}x'^{r}_{i}\right)dB^{r}_{tk} = \\ =\sqrt{\frac{\epsilon}{N}}\sqrt{\sum_{k=1}^{n}F_{ik}F_{ik}C^{N}_{jj}+F_{jk}F_{jk}C^{N}_{ii}+2F_{ik}F_{jk}C^{N}_{ij}}\;dB_t$$

and (1.10) becomes:

$$dC^{N}_{ij}=\sum_{k=1}^{n}\left(A_{ik}(X)C^{N}_{kj}+C^{N}_{ik}A^{T}_{kj}(X)+\epsilon F_{ik}F^{T}_{kj}\right)dt+ \\ +\sum_{k=1}^{n}\sqrt{\frac{\epsilon}{N}}R_{ik}(C^{N})\;dB_{tkj}\;, \tag{1.11}$$

where $dB_{tij}$ is an $n\times n$ matrix of infinitesimal increments of Brownian motion, and the elements of $R_{ij}$ are:

$$R_{ij}(C^{N})=\sqrt{Q_{ii}C^{N}_{jj}+Q_{jj}C^{N}_{ii}+2Q_{ij}C^{N}_{ij}}\;. \tag{1.12}$$

with $Q_{ij}=\sum_{k=1}^{n}F_{ik}F^{T}_{kj}$. Equations (1.8) and (1.11) which govern the evolution of the mean flow interacting with $N$ independent perturbation realizations will be referred to as the ensemble quasi-linear equations (EQL).

The stochastic term in the EQL vanishes as the number of realizations increases and in the limit $N\to\infty$ we obtain the autonomous and deterministic system of Stochastic Structural Stability theory (S3T) for the mean $X$ and the associated perturbation covariance matrix $C_{ij}=\lim_{N\to\infty}C^{N}_{ij}$:

$$\frac{dX_i}{dt}-\sum_{j,k}a_{ijk}X_jX_k+\sum_{j}b_{ij}X_j=\sum_{j,k}a_{ijk}\overline{C_{jk}}+F_i\;, \tag{1.13a}$$

$$\frac{dC_{ij}}{dt}=\sum_{k=1}^{n}\left(A_{ik}(X)C_{kj}+C_{ik}A^{T}_{kj}(X)\right)+\epsilon Q_{ij}\;. \tag{1.13b}$$

### 1.3 Remarks on the S3T system

1. We have followed a physically based derivation of the S3T equations as in Farrell and Ioannou (2003). These equations can also be obtained using Hopf's functional method (Hopf, 1952; Frisch, 1995) by truncating the cumulant expansion at second order producing the equivalent CE2 system (Marston et al., 2008).
2. Whether S3T provides an accurate model of a given turbulent flow depends on the appropriateness of the choice of averaging operator as well as the choice of the stochastic parameterization for the perturbation-perturbation interaction and any external perturbation forcing.
3. In the case of homogenous isotropic turbulence the stochastic excitation must be very carefully fashioned in order to obtain approximately valid statistics using a stochastic closure while in highly sheared flows the form of the stochastic excitation is not crucial so long as it is broadband. The reason is that in strongly sheared flows the operator $A_{ij}$ is highly non-normal and only a few perturbations structures are highly amplified. As a result the dynamics of the turbulence is essentially determined by interaction between the mean and these perturbations and is insensitive to the exact specification of the forcing so long as these structures are excited.
4. The S3T dynamics exploits the idealization of an infinite ensemble of perturbations interacting with the mean. It follows that S3T becomes increasingly accurate as the number of effectively independent perturbations contributing to influence the mean increases.
5. It is often the case that the zonal mean is an attractive choice for the averaging operator. A stable fixed point of the associated S3T system then corresponds to a statistical turbulent state comprising a mean zonal jet and fluctuations about it with covariance $C_{ij}$ so that perturbation $x'_1,\ldots x'_n$ is predicted to occur with probability $p(x'_1,\ldots,x'_n)=\exp(-1/2\sum_{i,j}(\mathbf{C}^{-1})_{ij}x'_ix'_j)/\sqrt{(2\pi)^n\det(\mathbf{C})}$.
6. S3T theory has also been applied to problems in which a temporal rather than a spatial mean is appropriate. The interpretation of the ensemble mean is then as a Reynolds average over an intermediate time scale, in which interpretation the perturbations are high frequency motions while the mean constitutes the slowly varying flow components (Bernstein and Farrell, 2010; Bakas and Ioannou, 2013a).
7. Often the attractor of the S3T dynamics is a fixed point representing a regime with stable statistics. However, the attractor of the S3T dynamics need not be a fixed point and in many cases a stable periodic orbit emerges as the attracting solution. In many turbulent systems large scale observables exhibit slow and nearly periodic fluctuation despite short intrinsic time scales for the turbulence and the lack of external forcing to account for the long time scale (i.e. the Quasi Biennial Oscillation in the Earth's atmosphere, the solar cycle). S3T provides a mechanism for such phenomena as reflections of a limit cycle attractor of the ideal S3T dynamics.
8. When rendered unstable by change of a system parameter, these equilibria predict structural reorganization of the whole turbulent field which may lead to establishment of a new stable statistical mean state. For example, S3T dynamics predicts bifurcation from the statistical homogeneous regime in which there are no zonal flows to a statistical regime with zonal flows when a parameter changes or predicts the transition from a regime characterized by two jets to a regime with a single jet.
9. The EQL equations (1.8) and (1.11) contain information about the fluctuations remaining in the ensemble dynamics when the number of ensemble members is finite. These fluctuation statistics determine the statistics of noise induced transitions between ideal S3T equilibria.

10. The close correspondence of S3T and NL simulations suggests that turbulence in shear flow can be essentially understood as the quasi-linear interaction between a spatial or temporal mean flow and perturbations.
11. The S3T system has bounded solutions and if destabilized typically equilibrates to a fixed point which can be identified with statistically stable states of turbulence (Farrell and Ioannou, 2003). Moreover, these equilibria closely resemble observed statistical states. For example S3T applied to an unstable baroclinic flow takes the form of baroclinic adjustment that is observed to occur in observations and in simulations (Stone and Nemet, 1996; Schneider and Walker, 2006; Farrell and Ioannou, 2008, 2009c).

## 1.4 Applying S3T to study SSD equilibria and their stability

S3T dynamics comprises interaction between the mean flow, $X$, and the turbulent Reynolds stress obtained from the second order cumulants of the perturbation field, $C$, associated with it. A fixed point of this system, when stable, corresponds to a realizable stationary statistical mean turbulent state. When rendered unstable by change of a system parameter, these equilibria predict structural reorganization of the whole turbulent field leading to establishment of a new statistical mean state. These bifurcations correspond to a new type of instability in turbulent flows associated with statistical mean state reorganization. Although such reorganizations have been commonly observed there has not heretofore been a theoretical method for analyzing or predicting them.

We consider first stability of an equilibrium probability distribution function in the context of S3T dynamics. The S3T equilibrium is determined jointly by an equilibrium mean flow $X^e$ and a perturbation covariance, $C^e$, that together constitute a fixed point of the S3T equations (1.13a) and (1.13b):

$$\sum_{j,k} a_{ijk} X^e_j X^e w_k - \sum_j b_{ij} X^e_j + \sum_{j,k} a_{ijk} \overline{C^e_{jk}} + F_i = 0 \ , \tag{1.14a}$$

$$\sum_k \left( A_{ik}(X^e) C^e_{kj} + C^e_{ik} A^T_{kj}(X^e) \right) + \epsilon Q_{ij} = 0 \tag{1.14b}$$

The linear stability of a fixed point statistical equilibrium $(X^e, C^e_{ij})$ is determined by the equations

$$\frac{d\delta X_i}{dt} = \sum_k A_{ik}(X^e)\delta X_k + \sum_{j,k} a_{ijk} \overline{\delta C_{jk}} \ , \tag{1.15a}$$

$$\frac{d\delta C_{ij}}{dt} = \sum_k \Big( \delta A_{ik} C^e_{kj} + C^e_{ik} \delta A^T_{kj} + + A_{ik}(X^e)\delta C_{kj} + \delta C_{ik} A^T_{kj}(X^e) \Big) \ , \tag{1.15b}$$

with

$$\delta A_{ij} = \sum_k \left( a_{ikj} + a_{ijk} \right) \delta X_k \ . \tag{1.16}$$

The asymptotic stability of such a fixed point is determined by assuming solutions of the form $(\widehat{\delta X}_i, \widehat{\delta C}_{ij}) e^{\sigma t}$ with $\delta A_{ij} = \widehat{\delta A}_{ij} e^{\sigma t}$ and by determining the eigenvalues, $\sigma$, and the eigenfunctions of the system:

$$\sigma \widehat{\delta X}_i = \sum_k A_{ik}(X^e) \widehat{\delta X}_k + \sum_{j,k} a_{ijk} \overline{\widehat{\delta C}_{jk}} \ , \tag{1.17a}$$

$$\sigma \widehat{\delta C}_{ij} = \sum_k \Big( \widehat{\delta A}_{ik} C^e_{kj} + C^e_{ik} \widehat{\delta A}^T_{kj} + + A_{ik}(X^e) \widehat{\delta C}_{kj} + \widehat{\delta C}_{ik} A^T_{kj}(X^e) \Big) \ , \tag{1.17b}$$

If the attractor of the S3T is a limit cycle, as it happens in many cases, then (1.13) admit time varying periodic solutions $(X^p_i(t), C^p_{ij}(t))$ with period $T$. The S3T stability of this periodically varying statistical state is determined by obtaining the eigenvalues of the propagator of the time dependent version of (1.15) over the period $T$.

## 1.5 Remarks on S3T instability

1. Consider an equilibrium mean flow $X^e$; if $\epsilon$ vanishes identically then $C^e$ also vanishes and S3T stability theory collapses to the familiar hydrodynamic instability of this mean flow, which is governed by the stability of $A(X^e)$. Consequently, S3T instability of $(X^e, 0)$ implies the hydrodynamic instability of $X^e$. However, if $\epsilon$ does not vanish identically then the instability of the equilibrium state $(X^e, C^e)$ introduces a new type of instability, which is an instability of the collective interaction between the ensemble mean statistics of the perturbations and the mean flow. It is an instability of the SSD and can be formulated only within this framework. Eigenanalysis of the S3T stability equations (1.15) provides a full spectrum of eigenfunctions comprising mean flows and covariances that can be ranked according to their growth rate. These eigenfunctions underly the behavior of QL and NL simulations. An example of this can be seen in the EQL system, governed by (1.8) and (1.11), which provides noisy reflections of the S3T equilibria and their stability. Specifically: the response of an EQL simulation near a stable S3T equilibrium manifests structures reflecting stochastic excitations of the S3T eigenfunctions by the fluctuations in EQL (Constantinou et al., 2014).
2. Hydrodynamic stability is determined by eigenanalysis of the $n \times n$ matrix $A(X^e)$. However, in order to determine the S3T stability of $(X^e, C^e)$ the eigenvalues of the $(n^2+n) \times (n^2+n)$ system of equations (1.15) must be found and special algorithms have been developed for this calculation (Farrell and Ioannou, 2003; Constantinou et al., 2014).
3. If $(X^e, C^e)$ is a fixed point of the S3T system, then $X^e$ is necessarily hydrodynamically stable, i.e. $A(X^e)$ is stable. This follows because the equilibrium covariance $C^e$ that

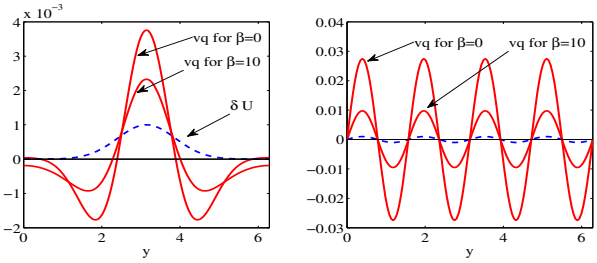


**Figure 1.1** Mean flow acceleration resulting when a small mean flow perturbation imposed on a background of turbulence forced by homogeneous broadband excitation. In the absence of mean flow the vorticity flux $\overline{v'q'} = 0$. The turbulence is distorted by the mean flow perturbation inducing vorticity fluxes that tend to amplify the imposed mean flow perturbation. In the left panel is shown the Gaussian mean flow perturbation together with the accelerations that are induced for $\beta = 0, 10$. The mean flow acceleration is not the same function as the $\delta U$ that was introduced. Right panel: when the $\delta U$ is sinusoidal the mean flow acceleration has the same sinusoidal form resulting in exponential growth leading to the emergence of large scale jets. Calculations were performed in a doubly periodic square beta plane box of length $2\pi$. The coefficient of linear damping is $r = 0.1$.

solves (1.14b) is determined from the limit

$$C^e_{ij} = \epsilon \lim_{t\to\infty} \int_0^t \sum_{k,l} e^{A(X^e)(t-s)}_{ik} \, Q_{kl} \, e^{A^T(X^e)(t-s)}_{lj} ds \ , \tag{1.18}$$

which does not exist if $A(X^e)$ is neutrally stable or unstable and consequently in either case $X^e$ is either case there is no realizable S3T equilibrium. This argument generalizes to S3T periodic orbits: if S3T has a periodic solution, $(X^p(t), C^p(t))$ of period $T$, then the perturbation operators $A(X^p(t))$ must be Floquet stable, i.e. the propagator over a period $T$ of $A(X^p(t))$ has eigenvalues, $\lambda$, with $|\lambda| < 1$, so that the time dependent mean states $X^p(t)$ are hydrodynamically stable.

4. While S3T stable solutions are necessarily also hydrodynamically stable, the converse is not true: hydrodynamic stability does not imply S3T stability. We will give examples below of hydrodynamically stable flows that are S3T unstable. This is important because it can lead to transitions between turbulent regimes that are the result of cooperative S3T instability rather than instability of the associated laminar flow.

## 1.6 Applying S3T to study the SSD of beta-plane turbulence

Consider a barotropic midlatitude beta-plane which models the dynamics of jet formation and maintenance in the Earth's upper troposphere or in Jupiter's atmosphere at cloud level. For simplicity assume a doubly periodic channel with $x$ and $y$ Cartesian coordinates along the zonal and the meridional direction respectively. The nondivergent zonal and meridional velocity fields are expressed in terms of a streamfunction, $\psi$, as $u = -\partial_y \psi$ and $v = \partial_x \psi$. The planetary vorticity is $2\Omega + \beta y$, with $\Omega$ the rotation rate at the channel's center. The relative vorticity is $q = \Delta\psi$ where $\Delta \equiv \partial^2_{xx} + \partial^2_{yy}$ is the Laplacian. The NL dynamics of this system is governed by the barotropic vorticity equation:

$$\partial_t q + u\,\partial_x q + v\,\partial_y q + \beta v = \mathcal{D} + \sqrt{\epsilon}\mathcal{F} \ . \tag{1.19}$$

The term $\mathcal{D}$ represents linear dissipation with the zonal component of the flow (corresponding to zonal wavenumber $k = 0$) dissipated at the rate $r_m$ while the non-zonal components are dissipated at rate $r > r_m$ (cf. Constantinou et al. (2014)). This dissipation specification allows use of Rayleigh damping while still modeling the physical effect of smaller damping rate at the large jet scale than at the much smaller perturbation scale. Periodic boundary conditions are imposed in $x$ and $y$ with periodicity $2\pi L$. Distances are nondimensionalized by $L = 5000$ km and time by $T = L/U$, where $U = 40\ \mathrm{m\,s^{-1}}$, so that the time unit is $T = 1.5$ day and $\beta = 10$ corresponds to a midlatitude value. Turbulence is maintained by stochastic forcing with spatial and temporal structure, $F$, and variance $\epsilon$.

Choosing as the averaging operator the zonal mean, i.e. $\overline{\phi}(y,t) = \int_0^{2\pi} \phi(x,y,t)\, dx/2\pi$ and decomposing the fields in zonal mean components and perturbations we obtain the discretized barotropic QL system:

$$\frac{dU}{dt} = \overline{v'q'} - r_m\, U \ , \tag{1.20a}$$

$$\frac{dq_k}{dt} = \mathbf{A}_k(U) q_k + \sqrt{\epsilon}\mathbf{F}_k dB_{tk} \ , \tag{1.20b}$$

where $U$ is the mean flow state and the subscript $k = 1, \ldots, N_k$, in (1.20b) indicates the zonal wavenumber and $q_k$ the Fourier coefficient of the perturbation vorticity that has been expanded as $q' = \Re\left(\sum_{k=1}^{N_k} q_k e^{ikx}\right)$. The $N_k$ wave numbers include only the zonal wavenumbers that are excited by the stochastic forcing, because with the specific choice of the averaging operator the $k \neq 0$ Fourier components do not directly interact in (1.20b) and therefore the perturbation response is limited to the wavenumbers directly excited by the stochastic forcing. The linear operator in (1.20b) evolving the perturbations is given by:

$$\mathbf{A}_k(U) = -ikU - ik(\beta - D^2 U)\Delta_k^{-1} - r \ , \tag{1.21}$$

with $\Delta_k = D^2 - k^2$, $\Delta_k^{-1}$ its inverse, and $D^2 = \partial_{yy}$. The continuous operator are discretized and approximated by matrices. The perturbation velocity appearing in (1.20a) is given by $v' = \Re\left(\sum_{k=1}^{N_k} ik\Delta_k^{-1} q_k e^{ikx}\right)$, and the meridional vorticity flux accelerating the mean flow is:

$$\overline{v'q'} = \sum_{k=1}^{N_k} \frac{k}{2} \mathrm{diag}\left(\Im\left(\Delta_k^{-1}\mathbf{C}_k\right)\right) \ , \tag{1.22}$$

with $\Im$ denoting the imaginary part, $\mathbf{C}_k = q_k q_k^\dagger$ the single ensemble member covariance, $\dagger$ the Hermitian transpose, and diag the diagonal elements of a matrix. The forcing structure is chosen to be non-isotropic with matrix elements:

$$F_{kij} = c_k \left[ e^{-(y_i - y_j)^2/(2s^2)} + e^{-(y_i - 2\pi - y_j)^2/(2s^2)} + \right.$$
$$\left. + \ e^{-(y_i + 2\pi - y_j)^2/(2s^2)} \right] , \tag{1.23}$$

with $s = 0.2/\sqrt{2}$ and the normalization constants chosen so that energy is injected at each zonal wavenumber $k$ at unit rate. The delta correlation in time of the excitation ensures that this energy injection rate is the same in the QL and NL simulations and is independent of the state of the system. This forcing is chosen to represent the forcing of the barotropic flow by baroclinic instability. For more details cf. Constantinou et al. (2014).

The barotropic S3T system becomes:

$$\frac{dU}{dt} = \sum_{k=1}^{N_k} -\frac{k}{2}\Im\left(\mathrm{diag}\left(\Delta_k^{-1}\mathbf{C}_k\right)\right) - r_m U \ , \qquad (1.24a)$$

$$\frac{d\mathbf{C}_k}{dt} = \mathbf{A}_k(U)\mathbf{C}_k + \mathbf{C}_k A_k^\dagger(U) + \epsilon\,\mathbf{Q}_k \ . \qquad (1.24b)$$

with $\mathbf{C}_k = \left\langle q_k q_k^\dagger \right\rangle$ and $\mathbf{Q}_k = \mathbf{F}_k\mathbf{F}_k^\dagger$. The imaginary part in (1.24a) requires that we add to the system an equation for the conjugate of the covariance. This is necessary for treating the S3T equations as a dynamical system and for analyzing the stability of S3T equilibria. Alternatively we can treat the real and imaginary part of the perturbation covariance as separate variables to obtain a real S3T dynamical system as in (1.13).

Under the assumption that the stochastic forcing in the periodic channel is homogeneous (1.24a) and (1.24b) admit the homogeneous equilibrium

$$U^e = 0 \quad , \quad \mathbf{C}_k^e = \frac{\epsilon}{2r}\mathbf{Q}_k \ , \qquad (1.25)$$

as shown in Appendix A. The assumption of the homogeneity of the forcing is crucial for obtaining the covariance (1.25), which is independent of $\beta$, and for obtaining a turbulent equilibrium with no flow, which requires that the excitation does not lead to any momentum flux convergence despite the presence of dissipation. If the excitation were confined to a latitude band, the homogeneous state could not be an S3T equilibrium. In that case, Rossby waves that originate from the region of excitation would dissipate in the far-field producing momentum flux convergence into the excitation region and acceleration of the mean flow there as demonstrated in section 3.2.1. The analysis that follows assumes that the forcing is homogeneous so that the homogeneous state (1.25) is an S3T equilibrium for all parameter values. The question is whether this homogeneous equilibrium is also S3T stable. If it becomes S3T unstable at certain parameter values this would be an example of a flow that is hydrodynamically stable but S3T unstable.

### 1.6.1 Formation and structural stability of beta-plane jets

To further motivate this possibility consider an infinitesimal perturbation of the mean flow, $\delta U$, as for example the one shown in Fig. 1.1a, and calculate the vorticity fluxes induced by this perturbation mean flow assuming that the turbulence adjusts adiabatically to $\delta U$ at each instant satisfying the equilibrium Lyapunov equations

$$\mathbf{A}_k(\delta U)\mathbf{C}_k + \mathbf{C}_k\mathbf{A}_k^\dagger(\delta U) = -\epsilon\mathbf{Q}_k \ , \qquad (1.26)$$

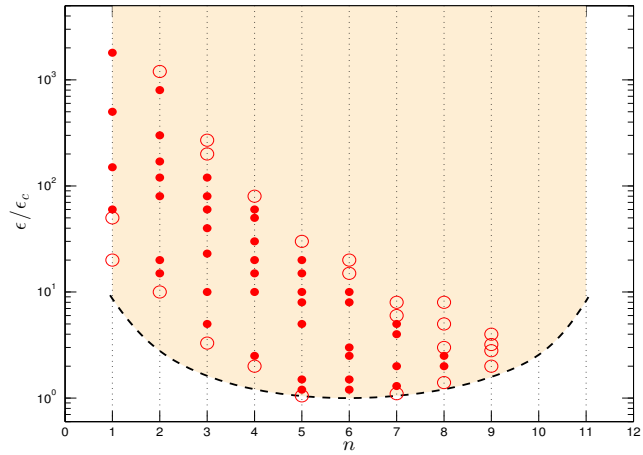


**Figure 1.2** S3T stability diagram showing the predicted zonal flow equilibria as a function of the number of jets, $n$, and the marginal fractional amplitude of excitation $\epsilon/\epsilon_c$ in the doubly periodic channel (dashed curve). The amplitude, $\epsilon_c$, is the minimal excitation amplitude, obtained from S3T stability analysis, that renders the homogeneous state unstable. For parameter values below the dashed curve the homogeneous state is S3T stable and no jets are predicted to emerge. Above the dashed curve the flow is S3T unstable and new statistical steady states emerge characterized by a different number of finite amplitude jets. S3T stable finite amplitude equilibrium jets are indicated with a full circle. Note that for given excitation amplitude there exist multiple S3T stable equilibria characterized by a different number of jets. With open circles we indicate unstable S3T equilibria determined with Newton iterations. Near the marginal curve S3T unstable modes do not equilibrate to stable finite amplitude S3T jet equilibrium as the same number of jets with the unstable eigenfunction due to inception of the universal Eckhaus instability as discussed in section 5.2.4 (also in Parker and Krommes (2013)). As the excitation amplitude increases jet mergers occur and stable S3T equilibria emerge with a smaller number of jets. Zonal wavenumbers $k = 1, \ldots, 14$ are forced, $\beta = 10$, $r = 0.1$, $r_m = 0.01$. (Courtesy of Navid Constantinou)

for $k = 1, \ldots, N_k$. By solving (1.26) we find that introducing the infinitesimal jet $\delta U$ results in an ensemble mean acceleration which can be calculated from (1.22). This induced acceleration, which is shown in Fig. 1.1a, is upgradient and tends to reinforce the mean flow perturbation that induced it, and this occurs even in the absence of $\beta$ (it vanishes for $\beta = 0$ only if the forcing covariance is isotropic). Repeated experimentation shows that this positive feedback occurs for any mean flow perturbation under any broadband excitation (isotropic or non-isotropic) as long as there is power at sufficiently high zonal wavenumbers[1]. This universal property of reinforcement of preexisting mean flow perturbations, revealed through S3T analysis, underlies the ubiquitous phenomenon of emergence of large scale structure in turbulent flows and explains why homogeneous equi-

[1] This implies that numerical simulations must be adequately resolved for jet formation to occur.

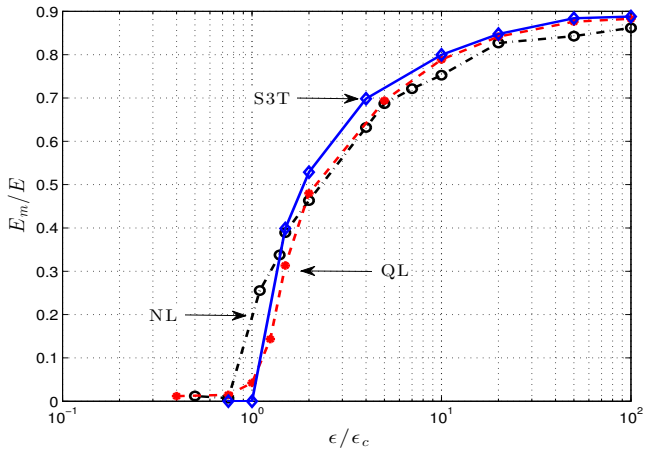


**Figure 1.3** The fraction of the energy of the zonal mean flow, $E_m$, to the total energy $E$, in S3T (solid and diamonds), QL (dashed and dots), and NL (dash-dot and circles) as a function of forcing amplitude $\epsilon/\epsilon_c$. S3T predicts that the homogeneous flow becomes unstable at $\epsilon/\epsilon_c = 1$ and a symmetry breaking bifurcation occurs at this forcing level whereupon zonal flows emerge. The predictions of S3T are reflected accurately in the sample integrations of QL and NL. The agreement between the NL and S3T argue that zonal jet formation is a bifurcation phenomenon and that S3T predicts both the inception of the instability and the finite equilibration of the emergent flows. Other parameters as in Fig. 1.2.

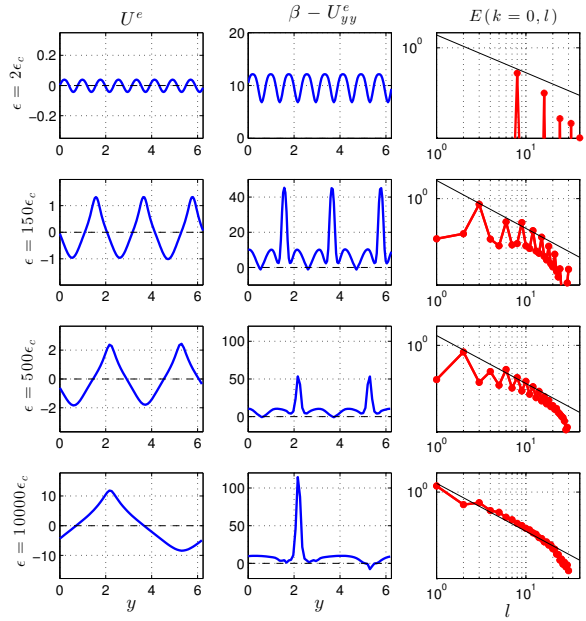


**Figure 1.4** Left: The equilibrium mean flow $U^e$ for excitation amplitudes $\epsilon/\epsilon_c = 2, 8, 150, 500, 10^4$. Center: the corresponding mean vorticity gradient $\beta - U^e_{yy}$. Right: The energy spectrum of the zonal mean flow. For the highly supercritical jets the energy spectrum approaches the approximate $l^{-5}$ dependence on the meridional wavenumber $l$ found in NL simulations. We argue that in the inviscid limit this slope should approach $l^{-4}$ as the prograde jet becomes non-differentiable. Other parameters as in Fig. 1.2. (Courtesy of Navid Constantinou)

librium states are unstable to jet perturbations[2]. The associated S3T modes, when unstable, give rise to finite amplitude jets, and when the homogeneous equilibrium is stable latent jets sporadically emerge and decay indicative of the presence of stochastically excited stable S3T modes. If there exists a mean flow perturbation that induces accelerations that have the same form as the imposed mean flow perturbation then this perturbation is an eigenfunction of the S3T stability equations that will grow or decay exponentially without change of form. S3T provides the framework for determining systematically the full spectrum of such eigenfunctions enabling full description of the evolution of a perturbation of small amplitude near an S3T equilibrium state.

Homogeneity in $y$ of the mean state assures that the mean flow component of the eigenfunctions of the S3T equilibrium (1.25) are $\delta U_n = \sin(ny)$, where $n$ indicates the number of jets associated with this eigenfunction. In Fig. 1.1b is shown a verification that a single harmonic induces mean flow acceleration of the same form and is therefore an eigenfunction of the S3T stability equations (1.15).

Consider the stability of the homogeneous equilibrium state (1.25) as a function of the excitation amplitude $\epsilon$ for a given coefficient of friction $r$. For $\epsilon = 0$ the equilibrium $U^e = 0$ and $\mathbf{C}^e_k = 0$ is S3T stable. For $\epsilon > 0$ the universal process of reinforcement of an imposed inhomogeneity occurs and therefore if $r_m = 0$ the homogeneous S3T equilibrium would immediately become unstable. For $r_m > 0$, instability occurs for $\epsilon > \epsilon_c$, where $\epsilon_c$ is the forcing amplitude that renders the S3T stability equation neutrally stable. The fractional critical forcing amplitude for the $n = 1, \ldots, 11$ S3T eigenfunctions is shown in Fig. 1.2. S3T predicts that for these parameters the maximum S3T instability occurs for mean flow perturbations $\delta U = \sin(ny)$ with $n = 6$ and thus S3T predicts that the breakdown of the homogeneous state occurs with the emergence of 6 jets in this channel.

### 1.6.2 Structure of jets in beta-plane turbulence

For parameter values exceeding those required for inception of the S3T instability the S3T attractor comprises statistical steady states with finite amplitude mean flows that can be characterized by their zonal mean flow index $E_m/E$, where $E_m$ is the kinetic energy density of the mean flow and $E$ to the total kinetic energy density of the flow, as in Srinivasan and Young (2012). A plot of $E_m/E$ as a function of forcing amplitude as predicted by S3T and as observed in QL and NL, is shown in Fig. 1.3 and the corresponding meridional structures of the jet equilibria for various parameter values are shown in Fig. 1.4. Jets corresponding to S3T equilibria must be hydrodynamically stable, which is associated with the mean vorticity gradient $\beta - U^e_{yy}$ of the equilibrium jets not changing sign in the case of sufficiently strong jets and as the coefficient of the linear damping be-

[2] The dynamics leading to this behavior in barotropic flows is discussed in Bakas and Ioannou (2013b). The counterpart of this process for three dimensional flows is discussed in Farrell and Ioannou (2012).

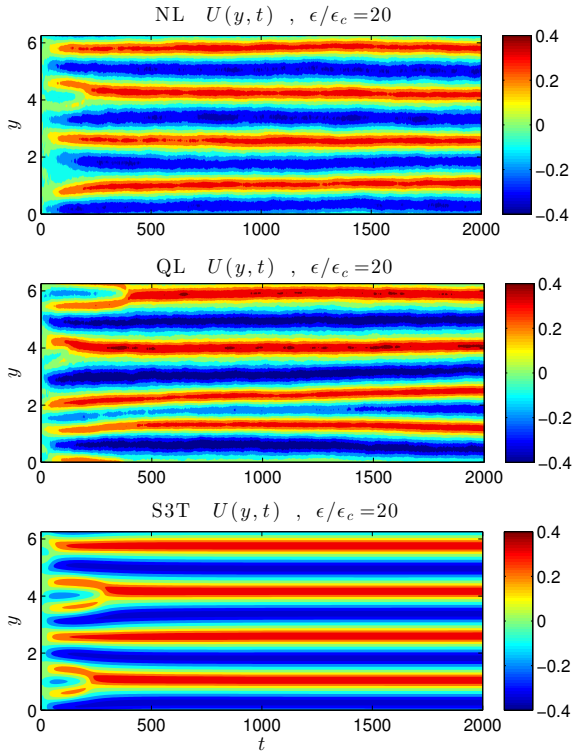


**Figure 1.5** Hovmöller diagrams of jet emergence in NL, QL and S3T simulations for the parameter value $\epsilon/\epsilon_c = 20$ of Fig. 1.3. Shown for the NL, QL and S3T simulations are $U(y,t)$. In all simulations the jet structure that first emerges is the $n = 6$ maximally growing jet structure predicted by S3T stability analysis. After a series of mergers S3T is attracted to a statistical steady state with a $n = 4$ jet. The whole process of jet mergers and S3T equilibration is accurately reflected in the sample QL and NL simulations. This figure shows that S3T predicts the structure, growth and equilibration of immoderately forced jets in both the QL and NL simulations. Other parameters as in Fig. 1.2.

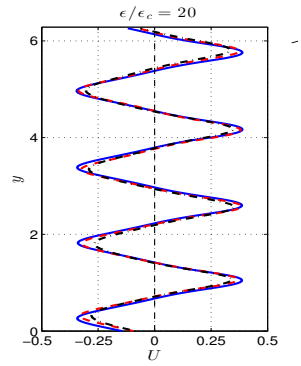


**Figure 1.6** The S3T equilibrium jet (solid-blue). This jet is a fixed point of the S3T system for $\epsilon/\epsilon_c = 20$, and its reflection in a NL simulation (dash-dot-black) and a QL simulation (dashed - red). The jets in NL and QL undergo small fluctuations as is evident in Fig. 1.5. In the figure we plot the average jet structure over ... units of time. This figure shows that S3T predicts the structure of immoderately forced jets in both the QL and NL simulations. Other parameters as in Fig. 1.2.

comes vanishingly small. Consistent with being constrained by this criterion, the equilibrated jets at high supercriticality shown in Fig. 1.4 assume the characteristic shape of sharply pointed prograde jets, with very large negative curvature, and smooth retrograde jets which satisfy $\beta \approx U^e_{yy}$. This consideration leads to the prediction that the mean spacing of the jets at high supercriticality is approximately given by $\sqrt{|U_{min}|/\beta}$, with $U_{min}$ the peak retrograde mean zonal velocity. At low supercriticality jet amplitude is too low for instability to be a factor in constraining jet structure and the jets equilibrate with nearly the structure of their associated eigenmode, as discussed in Farrell and Ioannou (2007). While this spacing of highly supercritical jets corresponds to the Rhines scaling, the mechanism that produces this scaling is associated with the modal stability boundary of the finite amplitude jet and is unrelated to the traditional interpretation of Rhines' scaling in terms of arrest of turbulent cascades.

S3T also predicts that the Fourier energy spectrum of the mean zonal flow of the highly supercritical jets has the approximate $l^{-5}$ dependence on the meridional wavenumber, $l$, in accord with highly resolved nonlinear simulations (Sukariansky et al., 2002; Danilov and Gurarie, 2004; Galperin et al., 2004) as well as in observations (Galperin et al., 2014). The finite amplitude jets that obtain in S3T are characterized by near discontinuity in the shear at the maxima of the prograde jets. This discontinuity would be consistent with a zonal energy spectrum proportional to $l^{-4}$. However, this discontinuity can not materialize in numerical simulations and it is rounded to give approximately the observed $l^{-5}$ dependence. Note that S3T not only predicts the energy spectrum of the zonal jets but in addition the structure and therefore the phase of the spectral components. The occurrence of this power law is theoretically anticipated by S3T because the upgradient fluxes act as a negative diffusion on the mean flow a result have the tendency to produce constant shear equilibria at each flank of the jet resulting in discontinuity in the derivative of the prograde jet (Farrell and Ioannou, 2007).

### 1.6.3 Comments on statistical equilibria in beta-plane turbulence

The emergence of jets as a bifurcation and the maintenance of jets as finite amplitude stable equilibria in barotropic turbulence are predictions of S3T that could not result from analysis within the NL and QL systems as in NL and QL turbulent states with stable statistics do not exist as fixed point equilibria so that a meaningful structural stability analysis of statistically stable equilibria states can not be performed. However, we show in Fig. 1.3, Fig. 1.5 and Fig. 1.6 that reflections of the bifurcation structure and of the finite amplitude equilibria predicted by S3T can be identified both in QL and NL sample simulations. The reflection in NL of the bifurcation structure predicted by S3T for $\epsilon \approx \epsilon_c$ is particu-

larly significant because it shows that the S3T perturbation instability faithfully reflects the physics underlying jet formation in turbulence as it manifests for infinitesimal mean flows. For a more detailed discussion cf. Constantinou et al. (2014).

## 1.7 Applying S3T to study SSD equilibria in baroclinic turbulence

A 2D barotropic fluid lacks a source term to maintain vorticity against dissipation and therefore it cannot self-sustain turbulence. Perhaps the simplest model that self-sustains turbulence is the baroclinic two-layer model, which is essentially two barotropic fluids sharing a horizontal boundary. We use this model to study the statistical dynamics of baroclinic turbulence. The eddy-eddy interactions that are neglected in S3T have been shown to be accurately parameterized in baroclinic turbulence by an additive stochastic excitation and the results reported here do not depend on this simplification (DelSole and Farrell, 1996; DelSole and Hou, 1999; DelSole, 2004b). The dynamics of baroclinic turbulence is studied using S3T with a state dependent closure in Farrell and Ioannou (2009c).

We consider the motion of a two layer fluid under quasi-geostrophic dynamics. The layers are of equal depth $H/2$ and bounded by horizontal rigid walls both at the bottom and the top. Variables of the top layer are denoted with the subscript 1, and of the bottom layer with subscript 2. The top layer density is $\rho_1$ and the bottom $\rho_2$ with $\rho_2 > \rho_1$ and the potential vorticity of each layer $q_i = \Delta\psi_i + \beta y + (-1)^i 2\lambda^2(\psi_1 - \psi_2)/2$ $(i = 1, 2)$, with $\lambda^2 = 2f_0^2/(g'H)$, where $g' = g(\varrho_2 - \varrho_1)/\varrho_1$ is the reduced gravitational acceleration, and $f_0$ the Coriolis parameter so that in terms of the Rossby radius of deformation $L_d = \sqrt{g'H}/f_0$, $\lambda = \sqrt{2}/L_d$. A constant temperature gradient is imposed in the meridional direction ($y$) which through the thermal wind relation induces, in the absence of turbulence and at equilibrium, a meridionally independent mean shear $U_T$ in the zonal ($x$) direction. This shear is taken without loss of generality to be expressed by zero velocity in the bottom layer (2) and a constant mean flow with stream function $U_T y$ in the top layer (1). The flow is relaxed through Newtonian cooling to the imposed flow and the bottom layer is dissipated by Ekman damping. The quasi-geostrophic dynamics governing this system is given by:

$$\partial_t q_1 + J(\psi_1, q_1) = \quad 2\lambda^2 r_T \frac{\psi_1 - \psi_2 - U_T y}{2} \tag{1.27}$$

$$\partial_t q_2 + J(\psi_2, q_2) = -2\lambda^2 r_T \frac{\psi_1 - \psi_2 - U_T y}{2} - r\Delta\psi_2 \ , \tag{1.28}$$

in which the advection of potential vorticity is expressed using the Jacobian $J(\psi, q) = \partial_x\psi\partial_y q - \partial_y\psi\partial_x q$, $r_T$ is the coefficient of the Newtonian cooling and $r$ is the coefficient of Ekman damping that acts only in the bottom layer. The above equations have been made non-dimensional with length scale $L_d = 1000$ km and time scale 1 d. With this scaling $\lambda = \sqrt{2}$, the velocity unit is 11.5 $\mathrm{ms}^{-1}$ and typical midlatitude values are $\beta = 1.4$. The above equations can be expressed in terms of the barotropic $\psi = (\psi_1 + \psi_2)/2$ and baroclinic $\theta = (\psi_1 - \psi_2)/2$ streamfunctions as:

$$\partial_t\Delta\psi + J(\psi, \Delta\psi) + J(\theta, \Delta\theta) + \beta\psi_x = -\frac{r}{2}\Delta(\psi - \theta) \tag{1.29}$$

$$\partial_t\Delta_\lambda\theta + J(\psi, \Delta_\lambda\theta) + J(\theta, \Delta\psi) + \beta\theta_x = \\ = \frac{r}{2}\Delta(\psi - \theta) + +2\lambda^2 r_T\left(\theta - \frac{U_T}{2}y\right) \tag{1.30}$$

where $\Delta_\lambda \equiv \Delta - 2\lambda^2$.

In order to apply periodic boundary conditions we follow Haidvogel and Held (1980) and decompose the barotropic and baroclinic streamfunctions into radiative equilibrium and deviations. The deviations are further decomposed into a zonal mean deviation (denoted with capitals) and deviations from the zonal mean deviation (which are referred to as perturbations) as:

$$\psi = -\frac{U_T}{2}y + \Psi + \psi' \quad , \qquad \theta = -\frac{U_T}{2}y + \Theta + \theta' \ . \tag{1.31}$$

With this decomposition we obtain the equations for the evolution of the zonal mean streamfunction deviations:

$$\partial_t D^2\Psi = -\overline{(J(\psi', \Delta\psi') + J(\theta', \Delta\theta'))} - \frac{r}{2}D^2(\Psi - \Theta) \tag{1.32a}$$

$$\partial_t D_\lambda^2\Theta = -\overline{(J(\psi', \Delta_\lambda\theta') + J(\theta', \Delta\psi'))} + \frac{r}{2}D^2(\Psi - \Theta) + 2\lambda^2 r_T\Theta \ , \tag{1.32b}$$

with $D^2 \equiv \partial_{yy}$ and $D_\lambda^2 \equiv D^2 - 2\lambda^2$ and the overline denotes zonal averaging. The corresponding barotropic and baroclinic components of the zonal mean flow deviations are $U^\psi = -\Psi_y$ and $U^\theta = -\Theta_y$. The equations for the evolution of the perturbations are:

$$\partial_t\Delta\psi' + \left(\frac{U_T}{2} + U^\psi\right)\partial_x\Delta\psi' + \left(\frac{U_T}{2} + U^\theta\right)\partial_x\Delta\theta' + \\ + (\beta - D^2U^\psi)\partial_x\psi' - D^2U^\theta\partial_x\theta' = -\frac{r}{2}\Delta(\psi' - \theta') + f_{NL}^\psi \ , \tag{1.33a}$$

$$\partial_t\Delta_\lambda\theta' + \left(\frac{U_T}{2} + U^\theta\right)\partial_x\Delta\psi' + \left(\frac{U_T}{2} + U^\psi\right)\partial_x\Delta_\lambda\theta' \\ + (\beta - D^2U^\psi)\partial_x\theta' + (\lambda^2U_T - D_\lambda^2U^\theta)\partial_x\psi' = \\ \frac{r}{2}\Delta(\psi' - \theta') + 2\lambda^2 r_T\theta' + f_{NL}^\theta \ , \tag{1.33b}$$

with the perturbation-perturbation interaction terms given by:

$$f_{NL}^\psi = \overline{(J(\psi', \Delta\psi') + J(\theta', \Delta\theta'))} - J(\psi', \Delta\psi') - J(\theta', \Delta\theta') \ , \tag{1.34a}$$

$$f_{NL}^\theta = \overline{(J(\psi', \Delta_\lambda\theta') + J(\theta', \Delta\psi'))} - J(\psi', \Delta_\lambda\theta') - J(\theta', \Delta\psi') \ . \tag{1.34b}$$

Equations (1.32) and (1.33) comprise the NL system that governs the two layer baroclinic flow. The corresponding QL system is obtained from the above equations by substituting for the perturbation-perturbation interaction a state independent and temporally delta correlated stochastic excitation with some added diffusive dissipation in order to obtain

an energy conserving closure (DelSole and Farrell, 1996; DelSole and Hou, 1999; DelSole, 2004b). We will impose periodic boundary conditions at the channel walls on $\Psi$, $\Theta$ , $\psi'$, $\theta'$ as in Haidvogel and Held (1980); Panetta (1993). These boundary conditions imply that the zonally and meridionally averaged velocity will at all times remain equal to that of the radiative equilibrium flow, which in turn implies that in this formulation periodic boundary conditions at the channel walls results in the temperature difference between the channel walls remaining fixed.

Under these assumptions the QL perturbation equations for the Fourier components of the barotropic and baroclinic streamfunction are:

$$\partial_t \psi_k = \mathbf{A}_k^{\psi\psi}\psi_k + \mathbf{A}_k^{\psi\theta}\theta_k + \sqrt{\epsilon}\Delta_k^{-1}\mathbf{F}_k\xi^{\psi}(t) \ , \tag{1.35a}$$

$$\partial_t \theta_k = \mathbf{A}_k^{\theta\psi}\psi_k + \mathbf{A}_k^{\theta\theta}\theta_k + \sqrt{\epsilon}\Delta_{k\lambda}^{-1}\mathbf{F}_k\xi^{\theta}(t) \ , \tag{1.35b}$$

in which we have assumed that the barotropic and baroclinic streamfunctions are forced respectively by $\sqrt{\epsilon}\Delta_k^{-1}\mathbf{F}_k\xi^{\psi}$ and $\sqrt{\epsilon}\Delta_{k\lambda}^{-1}\mathbf{F}_k\xi^{\theta}$. We also assume that $\xi^{\psi}$ and $\xi^{\theta}$ are independent temporally delta correlated stochastic processes of unit variance. The perturbation fields have been expanded as $\psi' = \Re\left(\sum_k \psi_k e^{ikx}\right)$ and $\theta' = \Re\left(\sum_k \theta_k e^{ikx}\right)$. The operators $\mathbf{A}_k$ linearized about the mean zonal flow $U = [U^{\psi}, U^{\theta}]^T$ are

$$\mathbf{A}_k(U) \ = \ \begin{pmatrix} \mathbf{A}_k^{\psi\theta} & \mathbf{A}_k^{\psi\theta} \\ \mathbf{A}_k^{\theta\psi} & \mathbf{A}_k^{\theta\theta} \end{pmatrix} \tag{1.36}$$

with :

$$\mathbf{A}_k^{\psi\psi} = \Delta_k^{-1}\left[-ik\left(\frac{U_T}{2}+U^{\psi}\right)\Delta_k - ik\left(\beta - D^2U^{\psi}\right)\right] - \frac{r}{2} \ , \tag{1.37a}$$

$$\mathbf{A}_k^{\psi\theta} = \Delta_k^{-1}\left[-ik\left(\frac{U_T}{2}+U^{\theta}\right)\Delta_k + ikD^2U^{\theta}\right] + \frac{r}{2} \ , \tag{1.37b}$$

$$\mathbf{A}_k^{\theta\psi} = \Delta_{k\lambda}^{-1}\left[-ik\left(\frac{U_T}{2}+U^{\theta}\right)\Delta_k - ik(\lambda^2U_T - D_\lambda^2U^{\theta}) + \right.$$
$$\left. + \frac{r}{2}\Delta_k\right] \ , \tag{1.37c}$$

$$\mathbf{A}_k^{\theta\theta} = \Delta_{k\lambda}^{-1}\left[-ik\left(\frac{U_T}{2}+U^{\psi}\right)\Delta_{k\lambda} - ik\left(\beta - D^2U^{\psi}\right)\right.$$
$$\left. - \ \frac{r}{2}\Delta_k + 2r_T\lambda^2\right] \ , \tag{1.37d}$$

and $\Delta_k \equiv D^2 - k^2$, $\Delta_{k\lambda} \equiv \Delta_k - 2\lambda^2$. Continuous operators are discretized and the dynamical operators approximated by finite dimensional matrices. The states $\psi_k$ and $\theta_k$ are represented by a column vector with entries the complex value of the barotropic and baroclinic streamfunction collocation points in $(y)$.

The corresponding S3T system is obtained by forming from the QL equations (1.35) the Lyapunov equation for the evolution for the zonally averaged covariance of the perturbation field which takes the form:

$$\frac{d\mathbf{C}_k}{dt} \ = \ \mathbf{A}_k(U)\mathbf{C}_k \ + \mathbf{C}_k\mathbf{A}_k^{\dagger}(U) \ + \ \epsilon\mathbf{Q}_k \ , \tag{1.38}$$

with the covariance for the wavenumber $k$ zonal Fourier component defined as:

$$\mathbf{C}_k \ = \ \begin{pmatrix} \mathbf{C}_k^{\psi\psi} & \mathbf{C}_k^{\psi\theta} \\ \mathbf{C}_k^{\psi\theta\dagger} & \mathbf{C}_k^{\theta\theta} \end{pmatrix} \ , \tag{1.39}$$

where $\mathbf{C}_k^{\psi\psi} = \langle \psi_k\psi_k^{\dagger} \rangle$ , $\mathbf{C}_k^{\psi\theta} = \langle \psi_k\theta_k^{\dagger} \rangle$, $\mathbf{C}_k^{\theta\theta} = \langle \theta_k\theta_k^{\dagger} \rangle$ with $\langle \bullet \rangle$ denoting zonal averaging. The covariance of the stochastic excitation

$$\mathbf{Q}_k \ = \ \begin{pmatrix} \Delta_k^{-1}\mathbf{F}_k\mathbf{F}_k^{\dagger}\Delta_k^{-1\dagger} & 0 \\ 0 & \Delta_{k\lambda}^{-1}\mathbf{F}_k^{\theta}\mathbf{F}_k^{\theta\dagger}\Delta_{k\lambda}^{-1\dagger} \end{pmatrix} \ , \tag{1.40}$$

has been normalized so for each $k$ a unit of energy per unit time is injected by the excitation and the amplitude of the excitation is controlled only by the parameter $\epsilon$.

The S3T equations for the mean flow (1.32) in terms of the perturbation covariances are:

$$\frac{dU^{\psi}}{dt} = \sum_k \ \frac{k}{2} \ \mathrm{diag}\left(\Im\left(\Delta_k C_k^{\psi\psi} + \Delta_k C_k^{\theta\theta}\right)\right) - \frac{r}{2}(U^{\psi} - U^{\theta}) \tag{1.41a}$$

$$\frac{dD_\lambda^2 U^{\theta}}{dt} = D^2 \sum_k \frac{k}{2} \ \mathrm{diag}\left(\Im\left(\Delta_{k\lambda} C^{\psi\theta\dagger} + \Delta_k C^{\psi\theta}\right)\right) +$$
$$+ \ \frac{r}{2}D^2(U^{\psi} - U^{\theta}) + 2\lambda^2 r_T U^{\theta} \ , \tag{1.41b}$$

As is the case in our previous barotropic examples, for homogeneous forcing there also exists a meridionally and zonally homogeneous turbulent S3T equilibrium state consisting of an equilibrium zonal mean flow equal to the radiatively imposed flow $U^e = [U_T/2, U_T/2]$ with $U^{\psi} = 0$ and $U^{\theta} = 0$ and a perturbation field with covariances, $\mathbf{C}_k^e$ which satisfy the corresponding steady state Lyapunov equations (1.38) (for the explicit expression of the equilibrium covariance see DelSole and Farrell (1995)). However, unlike the barotropic example, this homogeneous equilibrium state is feasible only for parameter values for which $U^e$ is hydrodynamically (baroclinically) stable. In the absence of dissipation instability occurs for this constant flow when $U_T > \beta/\lambda^2$ or in terms of the criticality parameter $\xi = \max(U_1 - U_2)\lambda^2/\beta$ when $\xi > 1$. This more general criticality parameter is customarily used despite the fact that $\xi > 1$ implies instability only when the flow is inviscid and meridionally uniform.

This equilibrium state exists only for $\Delta T < \Delta T_c$ in which case the mean flow is baroclinically stable. For $\Delta T > \Delta T_c$ only unstable laminar equilibria with $\epsilon = 0$ and $\mathbf{C}_k^e = 0$ exist and there are no homogeneous S3T equilibria for $\epsilon > 0$. We wish to examine the structural stability of the homogeneous S3T equilibria in the baroclinically stable regime with $\Delta T < \Delta T_c$ and to examine the finite amplitude structure of the S3T equilibria that exist in both the stable and unstable regimes. Because of the meridional homogeneity of the equilibrium state, the perturbation eigenfunctions are single harmonics. In Fig. 1.8 the critical values of stochastic forcing $\epsilon_c$ that render the eigenfunctions with $n = 1 - 4$ jets across the channel S3T unstable are plotted as a function of $\Delta T$. For $\Delta T > \Delta T_c$ the S3T equilibrium homogeneous states with $\epsilon = 0$ are hydrodynamically unstable and consequently also S3T unstable.

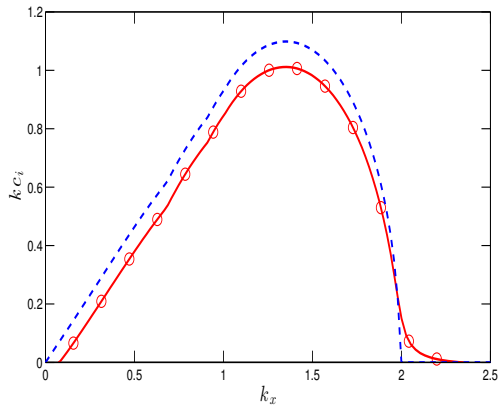


**Figure 1.7** The growth rate as a function of zonal wavenumber $k_x$ for the radiatively imposed baroclinic flow at supercriticality $\xi = 4$. The dashed curve is the growth rate is in the absence of any dissipation, in which case the shortwave cut-off occurs at $k_x = \lambda^2 = 2$. The solid line is for the dissipation parameters $r_T = 1/15$ and $r = 1/5$ used in the S3T calculations. With these dissipation parameters the flow becomes unstable for $\xi > \xi_c = 0.875$. The circles indicate the growth rate of the $k_x$ associated with the 14 harmonics used in the S3T calculations.

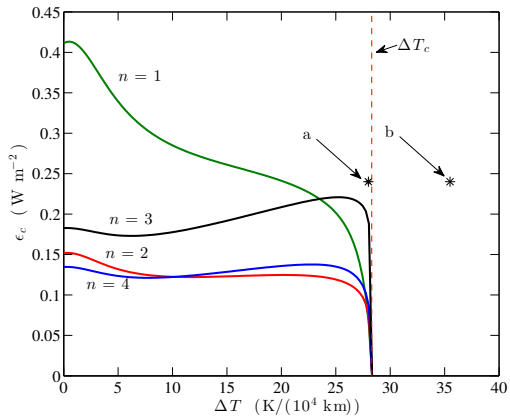


**Figure 1.8** The critical $\epsilon_c$ (Wm$^{-2}$ ) required to destabilize the the homogeneous S3T equilibrium state with $U_1^e = U_T$ and $U_2^e = 0$ as a function of the temperature difference $\Delta T$ across the channel. The different curves correspond to the critical forcing required for the S3T instability of the homogeneous state with mean flow eigenfunctions with meridional wavenumber $n = 1, .., 4$. The critical curves intercept the $\epsilon_c = 0$ axis at the critical $\Delta T_c$ for which the radiative equilibrium flow becomes baroclinically unstable. For $\Delta T > \Delta T_c$ the only homogeneous equilibrium states are the laminar states with $\mathbf{C}^e = 0$ and these are hydrodynamically and S3T unstable. Stars indicate the parameter values of the inhomogeneous equilibria shown in Fig. 1.9a,b. The eddy field comprises global zonal wavenumbers $1 - 14$.

The example case has a turbulent eddy field comprising the 14 gravest zonal wavenumbers in a doubly periodic channel with zonal ($x$) non-dimensional length 40 and meridional ($y$) width 10. The non-dimensional values of the dissipation parameters are $r_T = 1/15$, $r = 1/5$. As in section (1.4) the forcing structure $\mathbf{F}_k \mathbf{F}_k^\dagger$ has been chosen to have $(i, j)$ elements proportional to $\exp(-(y_i - y_j)^2/\delta^2)$, with $\delta = 0.5$ (corresponding to 500 km) producing strong localization of the stochastic forcing in space, and is normalized so that each $k$ injects 1 Wm$^{-2}$ into the flow. For temperature difference across the channel $\Delta T$ the radiatively equilibrium shear from thermal wind balance is $U_T = R\Delta T/f_0$, where $f_0 = 10^{-4}$ s$^{-1}$ is the Coriolis parameter and $R = 287$ Jkg$^{-1}$K$^{-1}$ is the gas constant. This equilibrium flow becomes baroclinically unstable for $\Delta T > \Delta T_c$, which with the above dissipation parameters is $\Delta T_c = 28.3$ K/(10$^4$km).

As is the case in our previous barotropic examples, there also exists a meridionally and zonally homogeneous turbulent S3T equilibrium state consisting of an equilibrium zonal mean flow $U^e = [U_T/2, U_T]$ (corresponding to $U_1^e = U_T$ and $U_2^e = 0$) and a perturbation field with covariances, $\mathbf{C}_k^e$ which satisfy the corresponding steady state Lyapunov equations (1.38). This equilibrium state exists only for $\Delta T < \Delta T_c$ in which case the mean flow is baroclinically stable. For $\Delta T > \Delta T_c$ only unstable laminar equilibria with $\epsilon = 0$ and $\mathbf{C}_k^e = 0$ exist and there are no homogeneous S3T equilibria for $\epsilon > 0$. We wish to examine the structural stability of the homogeneous S3T equilibria in the baroclinically stable regime with $\Delta T < \Delta T_c$ and to examine the finite amplitude structure of the S3T equilibria that exist in both the stable and unstable regimes. Because of the meridional homogeneity of the equilibrium state, the perturbation eigenfunctions are single harmonics. In Fig. 1.8 the critical values of stochastic forcing $\epsilon_c$ that render the eigenfunctions with $n = 1-4$ jets across the channel S3T unstable are plotted as a function of $\Delta T$. For $\Delta T > \Delta T_c$ the S3T equilibrium homogeneous states with $\epsilon = 0$ are hydrodynamically unstable and consequently also S3T unstable.

In direct analogy with emergence of jets in the barotropic problem, for the baroclinically stable equilibrium with $\Delta T < \Delta T_c$ the homogeneous turbulent state becomes structurally unstable when $\epsilon > \epsilon_c$ and zonal jets grow at first exponentially but ultimately equilibrate nonlinearly at finite amplitude to a meridionally varying non-homogeneous state with mean jet structure $U^e(y)$. For the baroclinically unstable regime $\Delta T > \Delta T_c$, the system transitions to a fully developed baroclinic turbulence regime and for $\epsilon$ sufficiently large the S3T system settles into meridionally non-homogeneous equilibria which are stable finite amplitude counterparts of the non-homogeneous jet equilibria that exist at the same $\epsilon$ in the baroclinically stable regime with $\Delta T < \Delta T_c$. However, the baroclinic turbulence produces the self-consistent $\epsilon$ that is required to maintain its observed variance. We have constructed a closure to determine this value of $\epsilon$ self-consistently (Farrell and Ioannou, 2009c) but for our purposes here it suffices to simply identify the operating point of the turbulence by selecting that value of $\epsilon$ which maintains the observed turbulence variance. This results in highly accurate simulation of the observed turbulence. Examples of equilibria $U^e(y)$ are shown in Fig. 1.9 for both a baroclinically stable case with $\Delta T < \Delta T_c$ and a baroclinically unstable case with $\Delta T > \Delta T_c$. In the latter case, which correspond to statistically steady states of fully developed baro-

clinic turbulence, as $\Delta T$ increases the nonlinear equilibria increase in amplitude and encroach on the stability boundary of the eddy dynamics. To avoid this instability the jets become increasingly east/west asymmetric with the eastward-portion equilibrating by zonal confinement (Ioannou and Lindzen, 1986; James, 1987; Roe and Lindzen, 1996), and the westward jets equilibrating more barotropically approximately close to the Rayleigh-Kuo stability boundary while maintaining substantial baroclinicity. These jets, while stable, are highly non-normal and support strong transient growth. This non-normal growth is succinctly summarized in Fig. 1.9 (c,d) by comparison between the Frobenius norm of the resolvent of the jet perturbation dynamics

$$||\mathbf{R}(\omega)||_F^2 = \sum_k \text{trace}\left(\mathbf{R}_k(\omega)\mathbf{R}_k(\omega)^\dagger\right) \ , \tag{1.42}$$

where

$$\mathbf{R}_k(\omega) = -(i\omega\mathbf{I} + \mathbf{A}_k(U^e))^{-1} \ , \tag{1.43}$$

and its equivalent normal counterpart, with resolvent the diagonal matrix, $\mathbf{S}_k$, of the eigenvalues of $\mathbf{A}_k$ :

$$\mathbf{R}_k^\perp(\omega) = -(i\omega\mathbf{I} + \mathbf{S}_k)^{-1} \ . \tag{1.44}$$

The square Frobenius norm of the resolvent shown as a function of frequency $\omega$ in Fig. 1.9 is the ensemble mean eddy streamfunction variance, $\langle|\psi|^2\rangle$, that would be maintained by white noise forcing of this equilibrium jet. Non-normality increases the maintained streamfunction variance$\langle|\psi|^2\rangle$, over that of the equivalent normal system $\langle|\psi^\perp|^2\rangle$ and the extent of this increase is a measure of the non-normality. The non-normality of the equilibria which is associated with both baroclinic and barotropic growth processes, increases as $\Delta T$ increases as shown in Fig. 1.9.

The maintained eddy streamfunction variance, $\langle|\psi|^2\rangle$, in the equilibrium jet and for comparison the eddy streamfunction variance, of the equivalent normal jet system, $\langle|\psi^\perp|^2\rangle$, as a function of the criticality measure of the equilibrated flow $\xi \equiv 4\max(U_1 - U_2)/(\beta L^2)$ is shown Fig. 1.10. The eddy variance maintained by the equilibrium jet increases as $\xi^4$ while the equivalent normal system eddy variance, $\langle|\psi^\perp|^2\rangle$, does not increase appreciably. This increase in variance with criticality is due to the increase in the non-normality of the equilibrated jet. The heat flux, which is proportional to $\langle\overline{\theta\partial_x\psi}\rangle$, exhibits a $\xi^7$ power law behavior implying an equivalent higher order thermal diffusion. While such power law behavior is recognized to be generic to strongly turbulent equilibria (Held and Larichev, 1996; Barry et al., 2002; Zurita-Gotor, 2007), it lacked comprehensive explanation in the absence of the SSD-based theory for the structure of the statistical equilibrium turbulent state and its concomitant non-normality that is provided by S3T. Coexistence of very high non-normality with modal stability (also referred to as a HOT (Highly Optimized Tolerance) state (Carlson and Doyle, 2002)) has been heretofore regarded as highly unlikely to occur naturally and such systems have been generally thought to result from engineering contrivance. In fact the goal of much of classical control theory is to suppress modal instability by designing stabilizing feedbacks. That this process of modal stability suppression sometimes resulted in modally stable systems that were at the same time highly vulnerable to disruption due to large transient growth of perturbation led to the more recent development of robust control theory which seeks to control transient growth associated with non-normality as well as modal stability (Doyle et al., 2009). A widely accepted argument for the necessity of engineering intervention to produce a system that is at the same time modally stable and highly non-normal follows from the observation that in the limit of increasing system non-normality, arbitrarily small perturbations to the dynamics result in modal destabilization. If the dynamics is expressed using a dynamical matrix, as we have done here, this vulnerability of the non-normal dynamics to modal destabilization finds expression in the pseudo-spectrum of the dynamical matrix (Trefethen and Embree, 2005). It is remarkable that the naturally occurring feedback between the zonal mean flow and the perturbations in turbulent systems produces a dynamical feedback control stabilization that maintains the system in a state of marginal modal stability coexisting with strong non-normaility and associated large transient growth.

In summary, we have provided an explanation for the observation that adjustment to stable but highly amplifying states exhibiting power law behavior for flux/gradient relations is characteristic of strongly supercritical turbulence. One consequence of stability coexisting with high non-normality in the Earth's midlatitude atmosphere is the association of cyclone formation with chance occurrence in the turbulence of optimal or near optimal initial conditions (Farrell, 1982, 1989; Farrell and Ioannou, 1993a; DelSole, 2004a). We have explained why a state of high non-normality together with marginal stability is inherent: it is because the SSD of turbulence maintains flow stability by adjusting the system to be in the vicinity of a specific stability boundary, which is identified with the fixed point of the S3T equilibrium, while retaining the high degree of non-normality of the system. Such a state of extreme non-normality coexisting with exponential stability is an emergent consequence of the underlying SSD of baroclinic turbulence and can only result from the feedback control mechanism operating in baroclinic turbulence which has been identified by SSD analysis using S3T.

## 1.8 Application of S3T to study the SSD of wall-bounded shear flow turbulence

Consider the canonical three dimensional laboratory plane Couette flow between walls with velocities $\pm U_w$. The streamwise direction is $x$, the wall-normal direction is $y$, and the spanwise direction is $z$. Lengths are non-dimensionalized by the channel half-width, $\delta$, and velocities by $U_w$, so that the Reynolds number is $R = U_w\delta/\nu$, with $\nu$ the coefficient of the kinematic viscosity. We take for our example a Couette flow in a doubly periodic channel of non-dimensional length $L_x$ in the streamwise direction and $L_z$ in the spanwise.

In the absence of turbulence the equilibrium solution is the laminar Couette flow with velocity components $(y, 0, 0)$ which has been shown to be hydrodynamically linearly sta-

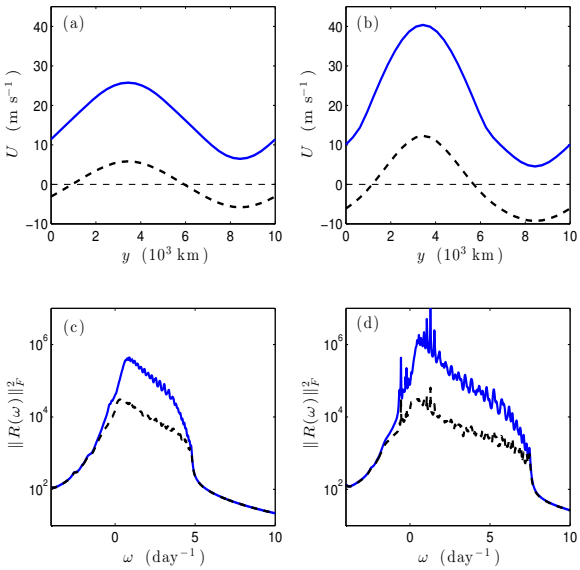


**Figure 1.9** Meridional structure of the equilibrium upper layer (continuous line) and lower layer (dashed line) mean flows maintained in a channel with mean thermal forcing $\Delta T = 28$ K/($10^4$ km) in (a) and $\Delta T = 35.5$ K/($10^4$ km) in (b). In (c) are shown the Frobenius norm of the resolvent associated with the eddy dynamics about mean flow (a) as a function of frequency and the Frobenius norm of the resolvent of the corresponding equivalent normal eddy dynamics (dashed). Similarly in (d) for the flow shown in (b). The eddy field comprises global zonal wavenumbers 1-14.

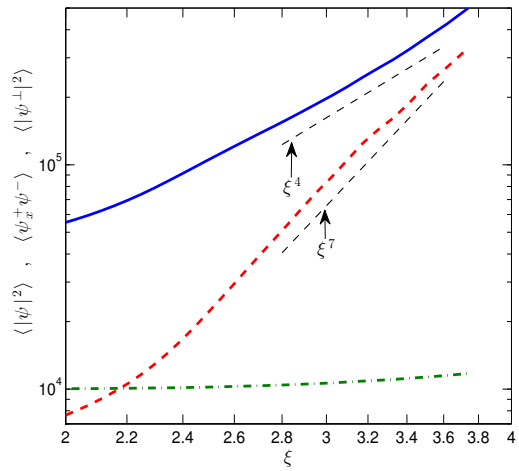


**Figure 1.10** For the equilibrated jets shown are: the eddy total streamfunction variance $\langle|\psi|^2\rangle$ (solid line) which is proportional to the geopotential height variance, $\langle\theta\partial_x\psi\rangle$ (dashed line) which is proportional to the eddy heat flux, and the variance maintained by the equivalent normal system $\langle|(\psi^\perp)^2\rangle$ (dash-dot line) as a function of the criticality parameter $\xi$. The flow shown in Fig. 1.9 a has $\xi = 2.5$, the flow in Fig. 1.9 b has $\xi = 3.51$. The eddy geopotential height variance increases as $\xi^4$, the heat flux increases as $\xi^7$, while the equivalent normal variance is nearly constant. Other parameters are as in the previous figure.

ble at all Reynolds numbers (Romanov, 1973) and globally stable for $R < 20.7$ (Joseph, 1966). However, experiments show that plane Couette flow can be induced by a perturbation to transition to a turbulent state for Reynolds numbers exceeding $R \approx 360$ (Tillmark and Alfredsson, 1992). During transition to turbulence and in the turbulent state a prominent large scale structure is observed in the flow. This structure, referred to as the roll/streak, comprises a modulation of the streamwise mean flow in the spanwise direction by regions of high and low velocity, referred to as streaks, together with a set of nearly cylindrical vortices in the wall-normal/spanwise plane, referred to as rolls. The roll circulation is such that the maximum negative wall-normal velocity is coincident with the maximum positive streamwise velocity of the streak and the maximum wall-normal velocity with the minimum streak velocity. This roll circulation serves to amplify the streak by advecting the mean shear; a mechanism referred to as lift-up. The streak is analogous to the jet that develops in barotropic and baroclinic flows. We will show that the roll-streak structure arises naturally from S3T instability of the spanwise homogeneous shear turbulence. To show this we formulate the S3T dynamics for this flow and demonstrate that the S3T homogeneous turbulent equilibria become unstable and the unstable eigenfunctions are the roll-streak structures.

Consider the vector velocity field $\vec{U}$ to be decomposed into a streamwise mean, with components, $(U, V, W)$, and deviation from this mean (the perturbation) with components $(u, v, w)$. The pressure gradient is similarly decomposed into its streamwise mean, $\nabla P$, and deviation from this mean, $\nabla p$. All streamwise averaged quantities are denoted with capitals and the streamwise averaging operation is denoted by an overline. In these variables a unit density fluid obeys the non-divergent Navier-Stokes equations:

$$\vec{u}_t + \vec{U}\cdot\nabla\vec{u} + \vec{u}\cdot\nabla\vec{U} + \nabla p - \Delta\vec{u}/R = -(\vec{u}\cdot\nabla\vec{u} - \overline{\vec{u}\cdot\nabla\vec{u}}) + \vec{e}\ , \tag{1.45a}$$

$$\vec{U}_t + \vec{U}\cdot\nabla\vec{U} + \nabla P - \Delta\vec{U}/R = -\overline{\vec{u}\cdot\nabla\vec{u}}\ , \tag{1.45b}$$

$$\nabla\cdot\vec{U} = 0\ \ ,\ \ \nabla\cdot\vec{u} = 0\ , \tag{1.45c}$$

with boundary conditions $\vec{u} = 0$ and $\vec{U} = (\pm 1, 0, 0)$ at $y = \pm 1$ and periodicity in $x$ and $z$.

In the perturbation equation (1.45a) allowance is made for specifying an explicit external perturbation forcing, $\vec{e}$. A stochastic parameterization is now introduced to account for both this external forcing and the perturbation-perturbation interactions, $\vec{u}\cdot\nabla\vec{u} - \overline{\vec{u}\cdot\nabla\vec{u}}$. With this parameterization, the perturbation equation becomes:

$$\vec{u}_t + \vec{U}\cdot\nabla\vec{u} + \vec{u}\cdot\nabla\vec{U} + \nabla p - \Delta\vec{u}/R = \vec{E}\ . \tag{1.46}$$

Perturbation equation (1.46), coupled with the mean flow equation, (1.45b), form the quasi-linear (QL) form of the Navier-Stokes equations. This approximate set of equations is also referred to as the restricted nonlinear (RNL) system (Thomas et al., 2014).

It is convenient to eliminate the pressure and express equation (1.46) in terms of cross-stream velocity $v$ and cross-stream vorticity, $\eta = \partial_z u - \partial_x w$. The equations then take

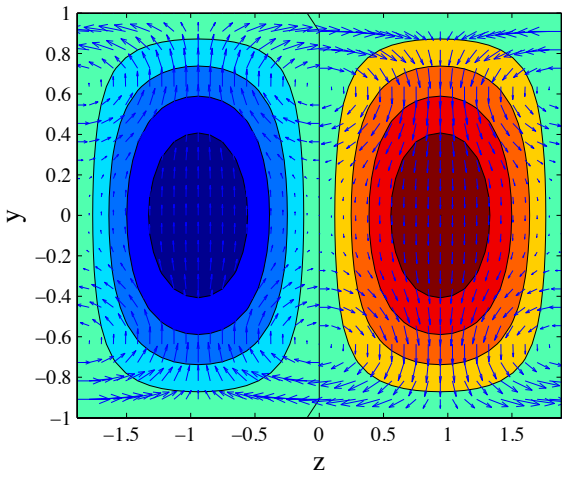


**Figure 1.11** The rate of change of streamwise roll acceleration induced by a streak perturbation to a Couette flow that is maintained turbulent by stochastic forcing. Distortion of the turbulence by the streak perturbation induces Reynolds stresses that force roll circulations supporting the streak via the lift-up mechanism. Shown are contours of the imposed streak perturbations, $\delta U = \cos(\pi y/2)\sin(2\pi z/L_z)$, with $\delta U > 0$ in $z > 0$, and vectors of the resulting rate of change of roll acceleration, $(\dot{V}, \dot{W})$. The Reynolds number is $R = 400$, $L_x = 1.75\pi$ and $L_z = 1.2\pi$.

the form:

$$\Delta v_t + U\Delta v_x + U_{zz}v_x + 2U_z v_{xz} - U_{yy}v_x - 2U_z w_{xy} - \\ -2U_{yz}w_x - \Delta\Delta v/R = \Delta E_v \ , \tag{1.47a}$$

$$\eta_t + U\eta_x - U_z v_y + U_{yz}v + U_y v_z + U_{zz}w - \\ -\Delta\eta/R = E_\eta \ . \tag{1.47b}$$

where $E_v$ and $E_\eta$ are the stochastic excitation in these variables (cf. Schmid and Henningson (2001)). In the perturbation equations (1.47), advection of perturbations by the small $V$ and $W$ components of the streamwise mean velocity has been neglected[3]. Using nondivergence the mean flow equation (1.45b) can be written as:

$$U_t = U_y\Psi_z - U_z\Psi_y - \partial_y\overline{uv} - \partial_z\overline{uw} + \Delta_1 U/R \ , \tag{1.48a}$$

$$\Delta_1\Psi_t = (\partial_{yy} - \partial_{zz})(\Psi_y\Psi_z - \overline{vw}) - \\ -\partial_{yz}(\Psi_y^2 - \Psi_z^2 + \overline{w^2} - \overline{v^2}) + \Delta_1\Delta_1\Psi/R \ . \tag{1.48b}$$

In (1.48b), $\Delta_1 \equiv \partial_{yy}^2 + \partial_{zz}^2$ and $V$ and $W$ have been expressed in terms of the streamfunction, $\Psi$, as $V = -\Psi_z$ and $W = \Psi_y$.

We next Fourier expand the perturbation fields in $x$: $v = \sum_k \hat{v}_k(y,z,t)e^{ikx}$ , $\eta = \sum_k \hat{\eta}_k(y,z,t)e^{ikx}$ and write the equations for the evolution of the Fourier components of

[3] The results presented are not affected by neglecting the advection of the perturbation field by $V$ and $W$ velocities in the perturbation equations cf. Thomas et al. (2014).

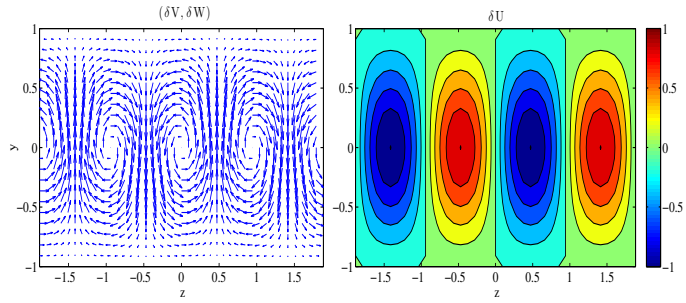


**Figure 1.12** The most unstable streamwise roll and streak eigenfunction of the S3T system linearized about the spanwise uniform equilibrium at supercriticality $\epsilon/\epsilon_c = 1.4$. The growth rate of this mode is $\lambda_r = 0.014$. Shown are velocity vectors $(\delta V, \delta W)$ (left) and streamwise velocity $\delta U$ (right). The ratio of the maxima of $(\delta U, \delta V, \delta W)$ is $(1, 0.06, 0.03)$. Other parameters are as in Fig. 1.11.

(1.47) in the matrix form

$$\frac{d\phi_k}{dt} = \mathbf{A}_k(U)\phi_k + \sqrt{\epsilon}\mathbf{F}_k dB_{tk} \ , \tag{1.49}$$

where the state of the system $\phi_k = [\hat{v}_k, \hat{\eta}_k]^T$ comprises the values of the $v_k$ and $\eta_k$ on the $N = N_y N_z$ grid points of the $(y,z)$ plane and

$$\mathbf{A}_k(U) = \begin{pmatrix} \mathbf{L}_{OS} & \mathbf{L}_{C_1} \\ \mathbf{L}_{C_2} & \mathbf{L}_{SQ} \end{pmatrix} \ , \tag{1.50}$$

with

$$\mathbf{L}_{OS} = \Delta^{-1}\left(-ikU\Delta + ik(U_{yy} - U_{zz}) - 2ikU_z\partial_z - \right. \\ \left. -2ik(U_z\partial_{yyz}^3 + U_{yz}\partial_{yz}^2)\Delta_2^{-1} + \Delta\Delta/R\right) , \tag{1.51a}$$

$$\mathbf{L}_{C_1} = 2k^2\Delta^{-1}\left(U_z\partial_y + U_{yz}\right)\Delta_2^{-1}, \tag{1.51b}$$

$$\mathbf{L}_{C_2} = U_z\partial_y - U_y\partial_z - U_{yz} + U_{zz}\partial_{yz}^2\Delta_2^{-1}, \tag{1.51c}$$

$$\mathbf{L}_{SQ} = -ikU\Delta + ikU_{zz}\Delta_2^{-1} + \Delta/R \ , \tag{1.51d}$$

being the conventionally designated Orr-Somerfeld, coupling, and Squire operators respectively. In equations (1.51), $\Delta^{-1}$ and $\Delta_2^{-1}$ are the inverses of the matrix Laplacians, $\Delta$ and $\Delta_2 = \partial_{xx}^2 + \partial_{zz}^2$, which are rendered invertible by enforcing the boundary conditions. The boundary conditions satisfied by the Fourier amplitudes of the perturbation fields are: periodicity in $x$ and $z$ and $\hat{v}_k = \partial_y\hat{v}_k = \hat{\eta}_k = 0$ at $y = \pm 1$ .

The ensemble average perturbation covariance, $\mathbf{C}_k = \langle\phi_k\phi_k^\dagger\rangle$, evolves according to the time-dependent Lyapunov equation:

$$\frac{d\mathbf{C}_k}{dt} = \mathbf{A}_k(U)\mathbf{C}_k + \mathbf{C}_k\mathbf{A}_k^\dagger(U) + \epsilon\mathbf{Q}_k \ , \tag{1.52}$$

in which: $\mathbf{Q}_k = \mathbf{F}_k\mathbf{F}_k^\dagger$. All the quadratic fluxes that enter into the streamwise averaged flow equations (1.48) become linear functions of the $\mathbf{C}_k$ and the mean flow evolution equa-

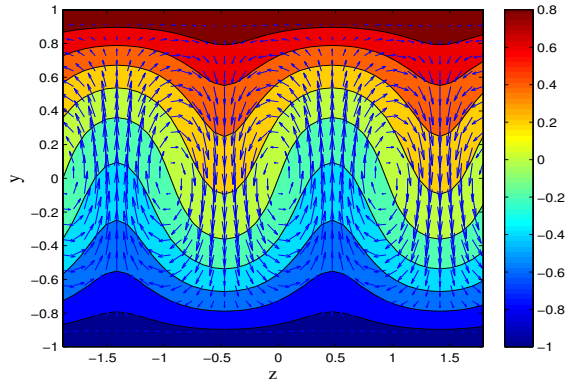


**Figure 1.13** The finite amplitude S3T equilibrium streamwise roll and streak resulting from the equilibration of the eigenmode shown in Fig. 1.12 at supercriticality $\epsilon/\epsilon_c = 1.4$. Shown are the streamwise averaged streamwise flow, $U(y,z)$, (contours) and the streamwise averaged velocities, $(V,W)$ (vectors). The maxima of the fields $(U,V,W)$ are $(0.26, 0.02, 0.009)$.

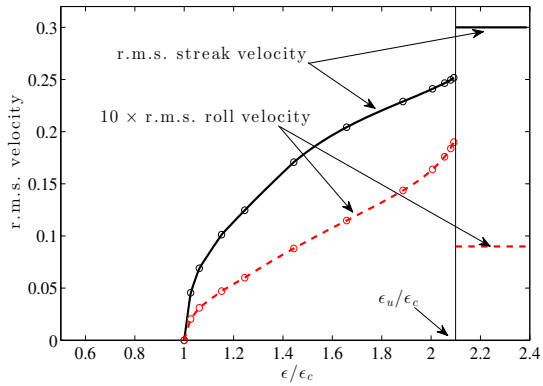


**Figure 1.14** Typical S3T bifurcation diagram for the Couette problem. Shown are the RMS streak velocity (solid) and 10× the RMS streamwise roll velocity (dashed) as a function of the perturbation forcing amplitude, $\epsilon$. For $\epsilon/\epsilon_c < 1$, the spanwise homogeneous state is S3T stable. At $\epsilon_c$ the spanwise uniform equilibrium bifurcates to an equilibrium with a streamwise roll and streak. Stable streamwise roll and streak equilibria extend up to $\epsilon_u/\epsilon_c = 2.1$ beyond which the streamwise roll and streak transitions to a time-dependent state which can self-sustain and the amplitudes of the roll and streak are independent of $\epsilon$. Shown for reference are the r.m.s. velocities of the streak and roll in the self-sustaining state. The Reynolds number is $R = 400$, $L_x = 1.75\pi$ and $L_z = 1.2\pi$.

tions (1.48) can be written concisely in the form:

$$\frac{d\Gamma}{dt} = G(\Gamma) + \sum_k \mathrm{Re}\left(\mathbf{L}_{RS}\mathbf{C}_k\right) \ , \tag{1.53}$$

where $\Gamma \equiv [U,\Psi]^T$ determines the three components of the streamwise averaged flow, the term $\sum_k \mathrm{Re}\left(\mathbf{L}_{RS}\mathbf{C}_k\right)$ produces by multiplying $\mathbf{C}_k$ with matrix $\mathbf{L}_{RS}$ the forcing of the mean equations by the perturbation field and $G(\Gamma)$ is the nonlinear term representing the self-advection of the streamwise averaged flow. Equations (1.52) and (1.53) comprise the S3T system for the Couette problem. The forcing covariances, $\mathbf{Q}_k$, are chosen to be spanwise homogeneous. Under this assumption spanwise homogeneous S3T equilibrium states exist. For further details on the formulation see Farrell and Ioannou (2012).

The Couette flow is a laminar equilibrium of the S3T system with excitation $\epsilon = 0$. For any $\epsilon$ and any spanwise homogeneous $Q_k$ there are always spanwise independent S3T equilibria having spanwise independent streamwise averaged flow $U_e(y)$ and $\Psi_e = 0$ and spanwise homogeneous perturbation covariances $\mathbf{C}_{ke}$. These are equilibria because, consistent with the spanwise independence of both the equilibrium mean flow and the imposed excitation, $\mathbf{C}_{ke}$ is also spanwise independent and this results in ensemble mean $\overline{uw}$, $\overline{v}^2$ and $\overline{w}^2$ that are independent of $z$, and $\overline{vw}$ that identically vanishes by symmetry. Consequently, (1.48b) admits $\Psi_e = 0$ as a solution as the ensemble mean perturbation forcing vanishes. However, the ensemble mean Reynolds stress divergence $\partial_y \overline{uv}$ in (1.48a) does not vanish and $U_e(y)$ satisfies $\Delta_1 U_e/R = \partial_y \overline{uv}$ indicating that the presence of external excitation induces a modification to the laminar Couette profile.

In analogy with the test function probe used to elucidate the mechanism underlying jet formation in barotropic flow (cf. section 1.6.1) we wish to determine the effect on the spanwise homogeneous field of turbulence of an infinitesimal spanwise-dependent mean-flow streak[4] perturbation $\delta U_s(y,z)$ added to the equilibrium flow, $U_e(y)$. We are particularly interested to find if the distortion of this turbulence results in a positive feedback on the perturbation streak, $\delta U_s(y,z)$. We determine this feedback by calculating the change $\delta\mathbf{C}_k$ in $\mathbf{C}_{ke}$ resulting from the streak perturbation $\delta U_s(y,z)$ as in the barotropic example. The divergence of the ensemble averaged perturbation Reynolds stresses resulting from this $\delta\mathbf{C}_k$ produce a torque resulting in forcing of a roll circulation according to equation (1.48b):

$$\partial_t \delta\Psi = \Delta_1^{-1}\left[-(\partial_{yy} - \partial_{zz})\ \delta\overline{vw} - \partial_{yz}\ (\delta\overline{w^2} - \delta\overline{v^2})\right] \ . \tag{1.54}$$

An example streak perturbations, $\delta U_s$, together with vectors of the induced streamwise roll velocity flow from (1.54), is shown in Fig. 1.11. Remarkably, this streak perturbation induces a distortion of the perturbation field resulting in a streamwise roll forcing configured to amplify the imposed streak perturbation through the lift-up mechanism i.e. positive wall-normal velocity is collocated with the minimum of the streak and maximum negative wall-normal velocity is collocated with the maximum of the streak. As a result this streak perturbation, when imposed on the initially homogeneous field of turbulence, induces Reynolds stresses driving a roll circulation producing through lift-up growth of the imposed streak. This robust Reynolds stress mediated destabilizing feedback process operating on the streamwise streak and roll structure has important implications for both

[4] The streak component, $U_s$, is in general defined as the departure of the streamwise averaged flow $U$ from its spanwise average $[U]$, i.e. $U_s = U - [U]$.

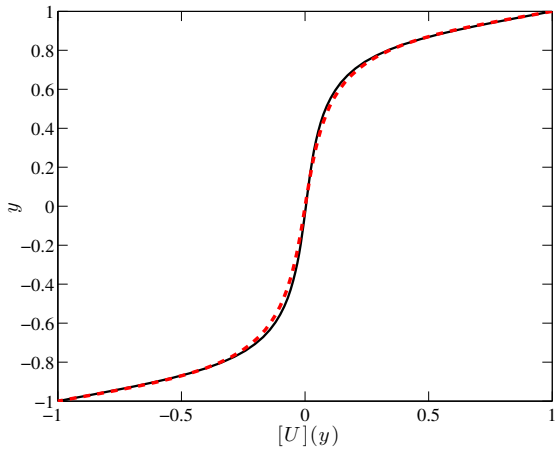


**Figure 1.15** Comparison of the spanwise and time averaged streamwise flow, $[U](y)$, for the self-sustaining state (solid) with the mean flow obtained from a $128 \times 65 \times 128$ direct numerical simulation (DNS) of Couette turbulence at $R = 1000$ in a doubly periodic channel in $x$ and $z$ of length $4\pi$ in each direction. The S3T self sustaining turbulent state produces on average a friction velocity based Reynolds number of $R_\tau = 64.9$ while the DNS simulation has $R_\tau = 66.2$ (this Reynolds number indicates the turbulent production and dissipation). This figure demonstrates that the S3T self-sustaining state produces a streamwise averaged flow profile consistent with simulations of Couette flow turbulence. (Courtesy of V. Thomas)

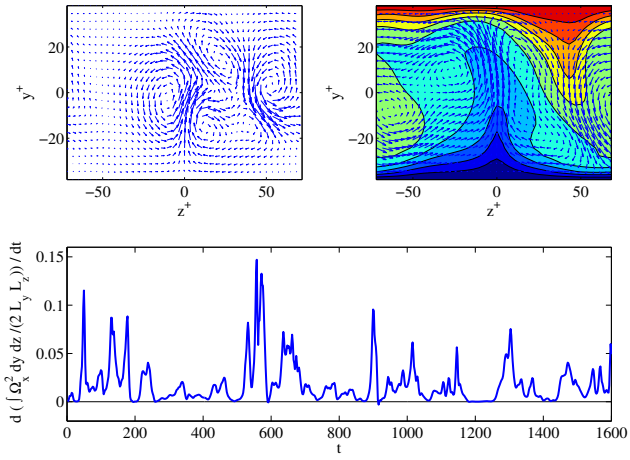


**Figure 1.16** Streamwise roll forcing by perturbation Reynolds stresses in the self-sustaining state for which $\epsilon = 0$. Top left: Vectors of instantaneous cross-stream/spanwise velocity acceleration, $(\dot{V}, \dot{W})$, at time t=980. Top right: Streamwise roll and streak structure at the same time. Lengths are measured in wall units. The spacing of the low velocity streaks in this self-sustaining state has the characteristic 100 wall unit spacing. Bottom: Time series of streamwise roll forcing as indicated by the rate of change of the average square streamwise vorticity. It is remarkable that the perturbations, in this highly time-dependent state, produce streamwise roll forcing, not only on average, but also at nearly every instant.

the transition to and the maintenance of turbulence in shear flows. We will show below that even when the streak structure is highly complex and time-dependent, as in a turbulent shear flow, the streamwise roll forcing produced by the perturbation Reynolds stresses remains collocated so as to amplify the streak. Moreover, this tendency of imposed streaks to induce, through the modification of the perturbation field, streamwise roll forcing with a tendency to reinforce the imposed streak provides the mechanism for a streamwise roll and streak plus turbulence cooperative instability in shear flow. This emergent instability is especially interesting because wall-bounded flows have laminar and turbulent mean velocity profiles with negative curvature and as a result do not support fast inflectional laminar flow instability. Most streak perturbations organize turbulent Reynolds stresses that do not exactly amplify the streak that produced them, as is clear in the case of the streak perturbation in Fig. 1.11. If a streak were to organize precisely the perturbation field required for its amplification then exponential modal growth of this streak and its associated streamwise roll and perturbation fields would result.

We determine now the S3T stability of the spanwise homogeneous equilibrium as a function of excitation amplitude, $\epsilon$, at a fixed Reynolds number, $R$, and show that exponentially unstable streamwise roll and streak modes arise in a spanwise independent field of forced turbulence if the perturbation forcing amplitude exceeds a threshold. The spanwise independent equilibrium is stable for $\epsilon < \epsilon_c$. At $\epsilon_c$ it becomes structurally unstable, while remaining hydrodynamically stable. The most unstable eigenfunction, which is shown in Fig. 1.12, consists of a roll circulation with a perfectly collocated streak. When this eigenfunction is introduced into the S3T system with small amplitude, it grows at first exponentially at the rate predicted by its eigenvalue and then asymptotically equilibrates at finite amplitude. This equilibrium solution, shown in Fig. 1.13, is a steady, finite amplitude streamwise roll and streak. The bifurcation diagram of the S3T equilibria is shown in Fig. 1.14 as a function of bifurcation parameter $\epsilon$. The finite amplitude streamwise roll and streak equilibria are S3T stable for $\epsilon_c \leq \epsilon \leq \epsilon_u$.

At $\epsilon_u$ there is a second bifurcation in which the equilibrium becomes S3T unstable, while remaining hydrodynamically stable, and the SSD fails to equilibrate, instead transitioning directly to a time-dependent state. Remarkably, the time-dependent S3T state that emerges for $\epsilon > \epsilon_u$ self-sustains even when $\epsilon$ is set to 0. This S3T self-sustaining time-dependent state produces realistic turbulence with mean turbulent profile $[U]$ shown in Fig. 1.15. Moreover, comparison with direct numerical simulations (DNS) verifies that this S3T turbulence is similar to Navier-Stokes turbulence despite the greatly simplified S3T dynamics underlying it (Thomas et al., 2014).

Remarkably, the S3T self-sustaining state naturally simplifies further by evolving to a minimal turbulent system in which the dynamics is supported by the interaction of the roll-streak structures with a perturbation field comprising small number (as few as 1) streamwise harmonics. This minimal self-sustaining turbulent system, which proceeds naturally from the S3T dynamics, provides a model self-

sustaining process (SSP) which can be understood with clarity. The basic ingredient of this self-sustained state is the robust tendency for streaks to organize the perturbation field so as to produce Reynolds stresses supporting the streak, via the lift-up mechanism as illustrated in Fig. 1.11. Although the streak is strongly fluctuating in the self-sustaining state, the tendency of the streak to organize the perturbation field is retained as illustrated in Fig. 1.16 in which a snapshot of the streamwise roll and streak is shown together with the associated roll acceleration, $(\dot{V}, \dot{W})$, arising from the perturbation Reynolds stresses (cf. equation (1.54)). The time derivative of the integral square streamwise vorticity, $d/dt(\int dydz\ \Omega_x^2)$ with $\Omega_x = W_y - V_z$, provides a measure of the torque produced by the Reynolds stress divergences that support the roll circulation. A times series of this diagnostic is also shown in Fig. 1.16. It is remarkable that the perturbations, in this highly time-dependent state, produce torques that maintain the streamwise roll not only on average but at nearly every instant. As a result, in this self-sustaining state, the streamwise roll is systematically maintained by the robust organization of perturbation Reynolds stress by the time-dependent streak that was identified by SSD analysis using the S3T system, while the streak is maintained by the streamwise roll through the lift-up mechanism. Through the resulting time-dependence of the roll-streak structure the constraint on instability imposed by the absence of inflectional instability in the mean flow is bypassed and the perturbation field is maintained by parametric growth, thus completing the SSP cycle[5].

We conclude that the dynamics of turbulence in wall-bounded shear flow can be understood at a fundamental level by using SSD and specifically by exploiting the direct relation between wall turbulence and the highly simplified S3T turbulence. Among the results obtained is that the mechanism of turbulence in wall bounded shear flow can be identified as the roll/streak/perturbation SSP that has been shown to maintain S3T turbulence.

## 1.9 Discussion

Although turbulence is commonly thought of as being definitional of disorder, the turbulent state in shear flow possesses an underlying order that is revealed by adopting statistical state variables to characterize the system instead of variables appropriate to single state realizations of the statistical mean turbulent state. This fundamental order at the center of turbulence dynamics has remained incompletely appreciated for lack of a conceptual basis as well as of methods for analyzing the order underlying statistical states of turbulence. In this review we have described an approach to understanding emergence of order in turbulence through adopting the perspective of SSD. From this perspective order is understood to arise in turbulence due to systematic cooperative interaction between large scale structures and the field of small scale turbulence in which these structures are embedded. Motivating examples of order emergence arise from considering a field of turbulence of some kind (GFD, MHD, Navier-Stokes) into which a trial perturbation of small amplitude but large scale is introduced. When introduced, such a structure would both alter the turbulence and be altered by it. Most such structures are dissipated by this interaction which is the basis for the concept of eddy viscosity. But suppose that we were to continue trying different large scale perturbations until we hit on a perturbation structure that affected the turbulence in just such a manner as to produce Reynolds stresses configured to amplify this structure without changing its form. Such a structure would naturally grow spontaneously out of the turbulence and would provide an explanation for the observed emergence of large scale structure in turbulent flow. This concept of coherent structure emergence through cooperative multi-scale interaction in turbulence takes analytical form through eigenanalysis of the SSD of the turbulence linearized about an equilibrium statistical state of the turbulence. Bifurcations occur in association with these instabilities that arise as parameters of the problem such as the amplitude of the turbulence excitation rate, the damping rate of the flow, or the beta parameter vary. Extensions of these perturbative instabilities into the nonlinear regime of the SSD reveal existence of fixed point equilibria that predict the structure of the associated finite amplitude coherent structures e.g. the zonal jets in the case of barotropic and baroclinic turbulence in planetary atmospheres. Moreover, these finite amplitude equilibria of the nonlinear SSD have an interpretation that transcends prediction of jet structure. The statistical state comprises both the mean flow and the perturbations which have mutually adjusted to produce the statistical state equilibrium so that these equilibria constitute a closure of the associated turbulence dynamics. The success of SSD in predicting the statistical mean state of turbulence as S3T equilibria in the systems we have discussed argues constructively that the nonlocal in spectral space interaction between perturbations and large scale mean flows that is retained in S3T captures the physical mechanism underlying the maintenance of the turbulent state in these systems. In addition, this closure is deterministic so that the physical mechanisms producing the closure are made available for study through analysis of the SSD underlying them. A straightforward example of such an insight into closure in turbulence arises in the case of barotropic beta-plane turbulence in which the observed jet scale in strong turbulence is linked mechanistically through SSD with Rayleigh's stability criterion; SSD analysis makes the further and associated verifiable prediction of successive bifurcations to jet structure of smaller wavenumber with increase in turbulence intensity. This example shows the power of SSD to both predict and provide physical explanation for observed phenomena as well as to predict new phenomena.

Adopting the perspective of SSD also provides conceptual insight into the dynamics of turbulence; an example of this is the concept of the dynamical trajectory of a statistical state. Consider a statistical state equilibrium consisting of a

[5] It has been shown that flows that at each time instant satisfy the necessary for stability Rayleigh condition can still become exponentially unstable if the flow is time dependent (cf. Farrell and Ioannou (1999)).

fixed point. An example might be a barotropic jet together with its supporting turbulence. This fixed point corresponds to a probability density function that is stationary in state space. But just as sample state trajectories, which are points in phase space, may converge to a fixed point or follow a time dependent path through the state space, so also statistical state trajectories may follow more or less intricate paths in phase space, taking their probability density function along with them. Interpretation of the dynamics of these statistical state trajectories provides a way to deepen understanding of the dynamic of turbulence. The successive jet wavenumber transitions leading to a lower and lower wavenumber for the equilibrium jet in strongly excited beta-plane turbulence mentioned above can be viewed as a trajectory of the deterministic SSD with the transitions understood as bifurcations associated with instability of the evolving statistical mean state, trajectories and instabilities that have no analytical counterpart in sample state dynamics. A familiar example of limit cycle behavior of a statistical state trajectory is provided by the QBO of the Earth's equatorial stratosphere which exhibits nearly periodic 27 month orbits in phase space. The analytical structure of the associated bifurcation only exists in the SSD framework (Farrell and Ioannou, 2003). Chaotic statistical state trajectories are found in jet dynamics of plasma turbulence (Farrell and Ioannou, 2009b). In the case of wall-bounded shear flow turbulence the statistical state trajectory is also chaotic and the time dependence of this statistical state consisting of the streak structure and the associated perturbations it supports, which results from their cooperative interaction, is a necessary condition for existence of the SSP maintaining the turbulence. This is because the turbulence is maintained by perturbations that result from parametric interaction with the streak, the time dependence of which is in turn maintained by interaction with the perturbations. This closed loop parametric process underlies energy transfer from the inflectionally stable forced mean flow that is required to maintain the turbulent state in wall-bounded shear flows is intrinsically a property of the SSD and this cooperative parametric process can only be understood through analysis of the dynamics of the statistical state of the turbulence.

Viewing turbulence from the perspective of SSD has proven to be remarkably tractable and to provide a richness of analysis and concept that has already allowed progress in a number of areas and holds promise of continuing insight into the nature of turbulence.

# APPENDIX

## 1 The homogeneous equilibrium covariance

To obtain that (1.25) is the equilibrium covariance under homogeneous stochastic excitation of a channel with periodic boundary conditions we use the property that $G_{k_x lm} = i\beta k_x \sum_\gamma \Delta^{-1}_{k_x lm}$ in $A_{k_x lm} = i\beta k_x \Delta^{-1}_{k_x lm} - r\delta_{lm}$ for $U^e = 0$ is antihermitian and then because $Q_{k_x lm}$ is Hermitian $\sum_{\gamma=1}^{n} \left( G_{k_x l\gamma} Q_{k_x \gamma m} + Q_{k_x l\gamma} G^\dagger_{k_x \gamma m} \right) = 0$ and (1.25) satisfies (1.24b) with no dependence on $\beta$. Consequently, the equilibrium covariance (1.25) retains the homogeneity of the forcing, and its associated mean vorticity flux can not accelerate the mean flow as any statistical quantity of a homogeneous field is spatially constant and the mean vorticity flux, which satisfies the Taylor identity: $\overline{v'q'} = -\partial_y(\overline{u'v'})$, vanishes.

This result can be more formally derived by making use of the property that in the matrix formulation of S3T in a periodic channel, in which the fields have been discretized on a grid, all matrices that correspond to homogeneous continuous operators as well as all covariances of homogeneous fields are circulant, i.e. each row is a cyclic shift of the row above it, because they commute with the matrix of spatial shifts on the grid lattice[6]. Consequently the forcing covariance at wavenumber $k_x$ must be of the form $Q_{k_x lm} = \sum_{k_y} Q_{k_x k_y} e^{ik_y(y_l - y_m)}$ with any choice of real and non-negative coefficients $Q_{k_x k_y}$, assuring in this way that $Q_{k_x lm}$ is positive definite, Hermitian and a covariance of a homogeneous field (this statement is the content of Bochner's theorem). Because for each $k_x$ we have

$$\sum_{m=1}^{n} \Delta^{-1}_{k_x \alpha m} Q_{k_x m\beta} = \sum_{k_y} Q_{k_x k_y} \sum_{m=1}^{n} \Delta^{-1}_{k_x \alpha m} e^{ik_y(y_m - y_\beta)}$$
$$= -\sum_{k_y} Q_{k_x k_y} \frac{e^{ik_y(y_\alpha - y_\beta)}}{k_x^2 + k_y^2}$$

we obtain that the diagonal elements of the homogeneous equilibrium $\sum_{m=1}^{n} \Delta^{-1}_{k_x \alpha m} C^e_{k_x m\beta}$ are equal and real and therefore the vorticity flux associated with the equilibrium covariance vanishes. In the argument above it was only required that the matrix multiplying the covariance is circulant having as eigenfunctions the harmonic $(e^{ik_y y_1}, \ldots, e^{ik_y y_n})$.

[6] Circulant matrices commute with each other and their common eigenbasis is a unitary matrix consisting of harmonics and they are very useful for exploring the properties of discrete S3T dynamics and stability in periodic channels (cf. Bakas and Ioannou (2011)).

# REFERENCES


Bakas, N. A., and Ioannou, P. J. 2011. Structural stability theory of two-dimensional fluid flow under stochastic forcing. *J. Fluid Mech.*, **682**, 332–361.

Bakas, N. A., and Ioannou, P. J. 2013a. Emergence of large scale structure in barotropic $\beta$-plane turbulence. *Phys. Rev. Lett.*, **110**, 224501.

Bakas, N. A., and Ioannou, P. J. 2013b. On the mechanism underlying the spontaneous emergence of barotropic zonal jets. *J. Atmos. Sci.*, **70**(7), 2251–2271.

Barry, L., Craig, G. C., and Thurbun, J. 2002. Poleward heat transport by the atmospheric heat engine. *Nature*, **415**, 774–777.

Bernstein, J., and Farrell, B. F. 2010. Low frequency variability in a turbulent baroclinic jet: Eddy–mean flow interactions in a two-level model. *J. Atmos. Sci.*, **67**(2), 452–467.

Brandt, L., Schlatter, P., and Henningson, D. S. 2004. Transition in boundary layers subject to free-stream turbulence. *J. Fluid Mech.*, **517**, 167–198.

Carlson, J. M., and Doyle, J. 2002. Complexity and Robustness. *Proc. Natl. Acad. Sci. USA*, **99 Suppl.**(1), 2538–2545.

Constantinou, N. C., Farrell, B. F., and Ioannou, P. J. 2014. Emergence and equilibration of jets in beta-plane turbulence: applications of Stochastic Structural Stability Theory. *J. Atmos. Sci.* doi:10.1175/JAS-D-13-076.1, in press.

Danilov, S., and Gurarie, D. 2004. Scaling, spectra and zonal jets in beta-plane turbulence. *Phys. Fluids*, **16**, 2592–2603.

DelSole, T. 2004a. The Necessity of Instantaneous Optimals in Stationary Turbulence. *J. Atmos. Sci.*, **61**, 1086–1091.

DelSole, T. 2004b. Stochastic models of quasigeostrophic turbulence. *Surveys in Geophysics*, **25**, 107–194.

DelSole, T., and Farrell, B. F. 1995. A stochastically excited linear system as a model for quasigeostrophic turbulence: Analytic results for one- and two-layer fluids. *J. Atmos. Sci.*, **52**, 2531–2547.

DelSole, T., and Farrell, B. F. 1996. The quasi-linear equilibration of a thermally mantained stochastically excited jet in a quasigeostrophic model. *J. Atmos. Sci.*, **53**, 1781–1797.

DelSole, T., and Hou, A. Y. 1999. Empirical stochastic models for the dominant climate statistics of a general circulation model. *J. Atmos. Sci.*, **56**, 3436–3456.

Diamond, P. H., Itoh, S-I., Itoh, K., and Hahm, T. S. 2005. Zonal flows in plasmas - a review. *Plasma Phys. Control. Fusion*, **47**, R35–R161.

Doyle, J. C., Francis, B. A., and R., Tannenbaum A. 2009. *Feedback Control Theory.* Dover Publications, New York.

Farrell, B. F. 1982. The initial growth of disturbances in a baroclinic flow. *J. Atmos. Sci.*, **39**, 1663–1686.

Farrell, B. F. 1989. Optimal excitation of baroclinic waves. *J. Atmos. Sci.*, **46**, 1193–1206.

Farrell, B. F., and Ioannou, P. J. 1993a. Stochastic dynamics of baroclinic waves. *J. Atmos. Sci.*, **50**, 4044–4057.

Farrell, B. F., and Ioannou, P. J. 1993b. Stochastic forcing of the linearized Navier-Stokes equations. *Phys. Fluids A*, **5**, 2600–2609.

Farrell, B. F., and Ioannou, P. J. 1999. Perturbation growth and structure in time dependent flows. *J. Atmos. Sci.*, **56**, 3622–3639.

Farrell, B. F., and Ioannou, P. J. 2003. Structural stability of turbulent jets. *J. Atmos. Sci.*, **60**, 2101–2118.

Farrell, B. F., and Ioannou, P. J. 2007. Structure and Spacing of Jets in Barotropic Turbulence. *J. Atmos. Sci.*, **64**, 3652–3665.

Farrell, B. F., and Ioannou, P. J. 2008. Formation of jets by baroclinic turbulence. *J. Atmos. Sci.*, **65**, 3353–3375.

Farrell, B. F., and Ioannou, P. J. 2009a. Emergence of Jets from Turbulence in the Shallow-Water Equations on an Equatorial Beta plane. *J. Atmos. Sci.*, **66**, 3197–3207.

Farrell, B. F., and Ioannou, P. J. 2009b. A Stochastic Structural Stability Theory model of the drift wave-zonal flow system. *Phys. Plasmas*, **16**, 112903.

Farrell, B. F., and Ioannou, P. J. 2009c. A Theory of Baroclinic Turbulence. *J. Atmos. Sci.*, **66**, 2444–2454.

Farrell, B. F., and Ioannou, P. J. 2012. Dynamics of streamwise rolls and streaks in turbulent wall-bounded shear flow. *J. Fluid Mech.*, **708**, 149–196.

Farrell, B. F., Gayme, D. F., Ioannou, P. J., Lieu, B. K., and Jovanovic, M. R. 2012. Dynamics of the roll and streak structure in transition and turbulence. Pages 43–54 of: *Studying Turbulence Using Numerical Simulation Databases - XIV*. Center of Turbulence Research. (online @ ctr.stanford.edu).

Frisch, U. 1995. *Turbulence: The Legacy of A. N. Kolmogorov.* Cambridge University Press.

Galperin, B., Nakano, H., Huang, H-P., and Sukoriansky, S. 2004. The ubiquitous zonal jets in the atmospheres of giant planets and Earth's oceans. *Geophys. Res. Lett.*, **31**, 13303–13308.

Galperin, Boris, Young, Roland M.B., Sukoriansky, Semion, Dikovskaya, Nadejda, Read, Peter L., Lancaster, Andrew J., and Armstrong, David. 2014. Cassini observations reveal a regime of zonostrophic macroturbulence on Jupiter. *Icarus*, **229**, 295 – 320.

Haidvogel, D. B., and Held, I. 1980. Homogeneous Quasi-Geostrophic Turbulence Driven by a Uniform Temperature Gradient. *J. Atmos. Sci.*, **37**, 2644–2660.

Held, I. M., and Larichev, V. D. 1996. A scaling theory for horizontally homogeneous, baroclinically unstable flow on a beta plane. *J. Atmos. Sci.*, **53**, 946–952.

Hopf, E. 1952. Statistical hydromechanics and functional calculus. *J. Ration. Mech. Anal.*, **1**, 87–123.

Ingersoll, A. P. 1990. Atmospheric dynamics of the outer planets. *Science*, **248**, 308–315.

Ioannou, P. J., and Lindzen, R. S. 1986. Baroclinic Instability in the Presence of Barotropic Jets. *J. Atmos. Sci.*, **43**, 2999–3014.

James, I. N. 1987. Suppression of Baroclinic Instability in Horizontally Sheared Flows. *J. Atmos. Sci.*, **44**(Dec.), 3710–3720.

Joseph, D. D. 1966. Nonlinear stability of the Boussinesq equations by the method of energy. *Arch. Rat. Mech. Anal.*, **22**, 163–184.

Kraichnan, R. H. 1959. The structure of isotropic turbulence at very high Reynolds numbers. *J. Fluid Mech.*, **5**, 497–543.

Lindzen, R. S. 1993. Baroclinic neutrality and the tropopause. *J. Atmos. Sci.*, **50**, 1148–1151.

Marston, J. B. 2010. Statistics of the general circulation from cumulant expansions. *Chaos*, **20**, 041107.

Marston, J. B. 2012. Atmospheres as Nonequilibrium Condensed Matter. *Annu. Rev. Condens. Matter Phys.*, **3**, 285–310.

Marston, J. B., Conover, E., and Schneider, T. 2008. Statistics of an unstable barotropic jet from a cumulant expansion. *J. Atmos. Sci.*, **65**, 1955–1966.

Øksendal, Bernt. 2000. *Stochastic Differential Equations*. Berlin: Springer-Verlag.

Orszag, S. A. 1977. Statistical Theory of Turbulence. In: Balian, R., and Peube, J. L. (eds), *Fluid Dynamics, Les Houches 1973*. Gordon and Breach, New York.

Panetta, R. L. 1993. Zonal jets in wide baroclinically unstable regions: persistence and scale selection. *J. Atmos. Sci.*, **50**, 2073–2106.

Parker, J. B., and Krommes, J. A. 2013. Zonal flow as pattern formation. *Phys. Plasmas*, **20**, 100703.

Roe, H. H., and Lindzen, R. S. 1996. Baroclinic adjustment in a two-level model with barotropic shear. *J. Atmos. Sci.*, **53**, 2749–2754.

Romanov, V. A. 1973. Stability of plane-parallel Couette flow. *Funct. Anal. Appl.*, **7**, 137–146.

Rose, H. A., and Sulem, P.-L. 1978. Fully developed turbulence and statistical mechanics. *J. Phys. France*, **39**, 441–484.

Schmid, P. J., and Henningson, D. S. 2001. *Stability and Transition in Shear Flows*. Springer, New York.

Schneider, T., and Walker, C. C. 2006. Self-organization of atmospheric macroturbulence into critical states of weak nonlinear eddy-eddy interactions. *J. Atmos. Sci.*, **63**, 1569–1586.

Srinivasan, K., and Young, W. R. 2012. Zonostrophic instability. *J. Atmos. Sci.*, **69**(5), 1633–1656.

Stone, P. H., and Nemet, B. 1996. Baroclinic Adjustment: A Comparison between Theory, Observations, and Methods. *J. Atmos. Sci.*, **53**, 1663–1674.

Sukariansky, S., Galperin, B., and Dikovskaya, N. 2002. Universal spectrum of two dimensional turbulence on rotating sphere and some basic features of atmospheric circulations on giant planets. *Phys. Rev. Lett.*, **89**, 124501–4.

Thomas, V., Lieu, B. K., Jovanović, M. R., Farrell, B. F., Ioannou, P. J., and Gayme, D. F. 2014. Self-sustaining turbulence in a restricted nonlinear model of plane Couette flow. *Phys. Fluids*. (submitted).

Tillmark, N., and Alfredsson, P. H. 1992. Experiments on transition in plane Couette flow. *J. Fluid Mech.*, **235**, 89–92.

Tobias, S. M., Dagon, K., and Marston, J. B. 2011. Astrophysical fluid dynamics via direct numerical simulation. *Astrophys. J.*, **727**, 127.

Trefethen, L. N., and Embree, M. 2005. *Spectra and Pseudospectra: The Behavior of Nonnormal Matrices and Operators*. Princeton University Press, Princeton.

Zurita-Gotor, P. 2007. The relation between baroclinic adjustment and turbulent diffusion in the two-layer model. *J. Atmos. Sci.*, **64**, 1284–1300.